Atmos. Chem. Phys. Discuss., doi:10.5194/acp-2015-946, 2016
Manuscript under review for journal Atmos. Chem. Phys.
Published: 23 February 2016

Atmospheric Chemistry and Physics Discussions

A comparison of sea salt emission parameterizations in Northwestern Europe using a chemistry transport model setup

Neumann Daniel[1], Matthias Volker[1], Bieser Johannes[1,2], Aulinger Armin[1], and Quante Markus[1]

[1]Helmholtz-Zentrum Geesthacht, Institute of Coastal Research, Max-Planck-Straße 1, 21502 Geesthacht, Germany
[2]Deutsches Zentrum für Luft- und Raumfahrt, Institute of Atmospheric Physics, Münchener Straße 20, 82234 Weßling, Germany

Correspondence to: daniel.neumann@hzg.de

Abstract. Atmospheric sea salt particles affect chemical and physical processes in the atmosphere. They provide surface area for condensation and reaction of nitrogen, sulfur, and organic species and are a vehicle of transport for these species. Additionally, HCl is released from sea salt. Hence, sea salt has a relevant impact on air quality, particularly in coastal regions with high anthropogenic emissions such as in the North Sea region. Therefore, the integration of sea salt emissions in modeling studies in these regions is necessary. However, it was found that sea salt concentrations are not represented with necessary accuracy in some situations.

In this study, three sea salt emission parameterizations depending on different combinations of wind speed, salinity, sea surface temperature, and wave data were implemented and compared: GO03 (Gong, 2003), SP13 (Spada et al., 2013), and OV14 (Ovadnevaite et al., 2014). The aim is to improve modeled atmospheric sea salt concentrations by identifying the parameterization that predicts the sea salt PM_{10} mass concentrations at different distances to the source regions most accurately and that represents atmospheric sea salt particle size distributions most appropriately in the region under consideration.

While the GO03 emissions yielded overestimations in the PM_{10} concentrations at coastal stations and underestimations of those at inland stations, OV14 emissions, vice versa, led to underestimations at coastal stations and overestimations at inland stations. Because of differently shaped particle size distributions of the GO03 and OV14 emission cases, the deposition velocity of the coarse particles differs between both cases which yields this distinct behavior at inland and coast stations. PM_{10} concentrations produced by the SP13 emissions generally overestimated measured concentrations. With respect to the size distribution, OV14 produced most accurate coarse particle concentrations, whereas GO03 produced most accurate fine particle concentrations. Overall, GO03 and OV14 produced most accurate results, but both parameterizations still reveal weaknesses in some situations.

1 Introduction

Sea salt particles affect atmospheric chemistry (Seinfeld and Pandis, 2006) and cloud formation. They are emitted as water droplets from the sea surface as a result of strong wind, the breaking of waves and the bursting of air bubbles. The parameterization of sea salt emissions has a long history (e.g., Blanchard and Woodcock, 1980; Fairall et al., 1983; Monahan and Muircheartaigh, 1980) because such parameterizations are necessary in chemistry transport models (CTMs) and climate models because of their

Atmos. Chem. Phys. Discuss., doi:10.5194/acp-2015-946, 2016
Manuscript under review for journal Atmos. Chem. Phys.
Published: 23 February 2016

Atmospheric Chemistry and Physics Discussions

impact on atmospheric processes. However, as shown by Gantt et al. (2015), Im (2013), and Neumann et al. (2015), sea salt concentrations are still not satisfactorily reproduced by CTMs in all situations; thus, improvements to sea salt emission parameterizations are necessary. Extensive reviews of sea salt emissions and emission parameterizations have been published in recent years (Lewis and Schwartz, 2004; de Leeuw et al., 2011; O'Dowd and de Leeuw, 2007; Spada et al., 2013).

Sea salt particles generated by the bursting of bubbles are the most relevant for atmospheric chemistry because they are smaller than sea salt particles produced by other processes and, thus, they have the longest atmospheric lifetime: Air is entrained into the sea water by the breaking of waves, which is primarily wind driven, and forms air bubbles, which then rise to the surface where they burst (Monahan et al., 1986). Organic surfactants at the surface, the sea surface temperature (SST) and the sea surface salinity (SAL) affect these processes (Martensson et al., 2003; Salter et al., 2015; Blanchard, 1964; Donaldson et al., 2006). A large number of parameterizations relating sea salt emissions to wind speed and other parameters have been published in recent decades. Several were derived from a wind-speed-based parameterization published by Monahan and Muircheartaigh (1980) and Monahan et al. (1986). Nevertheless, atmospheric sea salt concentrations are not always predicted with sufficient accuracy (Tsyro et al., 2011; Spada et al., 2013; Neumann et al., 2015), and improving these predictions remains an objective of ongoing research (Ovadnevaite et al., 2014; Gantt et al., 2015; Petelski et al., 2014; Salter et al., 2015; Long et al., 2011).

Sea salt particles provide a surface for the condensation of gaseous atmospheric species and for heterogeneous reactions. The dry deposition velocity of particles is dependent on size and differs from the dry deposition velocities of gases. Thus, the condensation of pollutants, such as nitric acid (HNO_3), sulfuric acid (H_2SO_4) and ammonia (NH_3), onto sea salt affects their atmospheric lifetimes and deposition patterns. The latter are important for quantifying the input of pollutants and nutrients into water bodies, e.g., for studying eutrophication. The condensation of strong acids (e.g., H_2SO_4 and HNO_3) onto sea salt particles reduces the pH of the particles, leading to the release of sea salt chloride (Cl^-) as hydrochloric acid (HCl) into the atmosphere. This HCl affects the ozone chemistry in polluted marine air by the release of Cl radicals through oxidation by OH radicals (Cai et al., 2008; Crisp et al., 2014; Knipping and Dabdub, 2003). The relevance of this process depends on the availability of atmospheric bases (e.g., NH_3), which increase the pH of the aerosols.

The North and Baltic Sea regions are areas of high anthropogenic activity giving rise to the emission of various air pollutants such as NOX, SO2, NH_3 and primary particulate matter, which lead to the formation of HNO_3, H_2SO_4 and secondary particulate matter. Sea salt plays an important role in affecting the deposition and heterogeneous chemistry of relevant pollutants in this air pollution regime. Thus, when modeling air pollution in Northwestern Europe, sea salt emissions must be adequately parameterized.

Therefore, the purpose of this study is to improve the modeling of atmospheric sea salt concentrations in Northwestern Europe by evaluating various open-ocean sea salt emission parameterizations. This is done by comparing three different sea salt emission parameterizations (Gong, 2003; Spada et al., 2013; Ovadnevaite et al., 2014) with each other and with measurements from stations within the network of the European Measurement and Evaluation Programme (EMEP). Gong (2003), which describes sea salt emissions by bubble bursting, is a widely used parameterization depending only on the wind speed. Spada et al. (2013) compared several parameterizations from which MA03/MO86/SM93 is used here. This parameterization depends on wind speed and SST. In addition to Gong (2003), Spada et al. (2013) describes the emission of spume droplets for high wind

Atmos. Chem. Phys. Discuss., doi:10.5194/acp-2015-946, 2016
Manuscript under review for journal Atmos. Chem. Phys.
Published: 23 February 2016

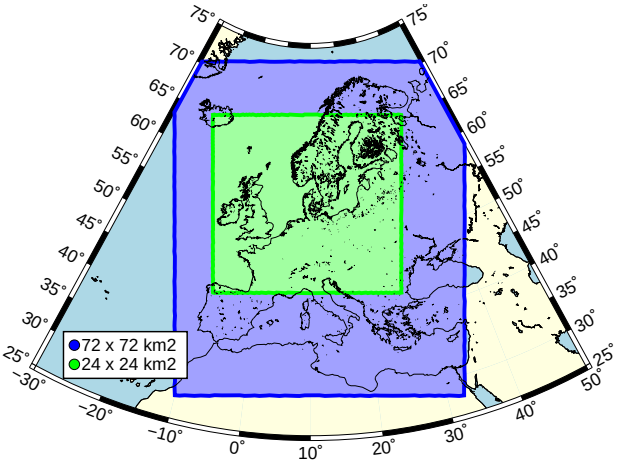

Figure 1. Study region and size of the model grids. The coarse grid (blue) includes Europe and parts of northern Africa. The first nested grid (green) includes Northwestern Europe, including the North and Baltic Seas.

speeds: Ovadnevaite et al. (2014) is a quite new parameterization that depends on wind speed, SST, SAL, and wave data and that should cover all sea salt production processes. It was not used in a CTM setup in the study region up till now. For this study, the parameterizations of Gong (2003) and Spada et al. (2013) were extended to depend on salinity.

There have been a few recent studies on sea salt in the Northwestern European region. Manders et al. (2010) evaluated sea salt measurements from various EMEP stations. Other studies addressed data from Mace Head (Cavalli et al., 2004; Ovadnevaite et al., 2014). Tsyro et al. (2011) compared five open ocean sea salt emission parameterizations, which depended on the wind speed only, in Europe. In this study comparing three sea salt emission parameterizations, the impact of SAL on sea salt particles generation as well as the contribution of surf zone emissions are considered. Additionally, with the employment of the parameterization of Ovadnevaite et al. (2014), an explicitly wave-dependent function is considered in this study.

2 Materials and Methods

2.1 Chemistry Transport Model

The simulations were performed using the Community Multiscale Air Quality (CMAQ) modeling system, which is developed and maintained by the U.S. EPA. Version 5.0.1 was used in this study. The study region was enclosed by a grid with dimensions of $24 \times 24\ \mathrm{km}^2$, which was one-way nested in a coarse grid with dimensions of $72 \times 72\ \mathrm{km}^2$ (Fig. 1). The outer boundary conditions were taken from TM5 model runs (Huijnen et al., 2010). The cb05tucl mechanism (Yarwood et al., 2005; Whitten et al., 2010; Tanaka et al., 2003; Sarwar et al., 2007) was used to represent the gas-phase chemistry, and the AERO05 mechanism (Nenes et al., 1998, 1999) was used to represent the particle-phase chemistry. CMAQ also includes in-cloud chemistry.

The aerosol phase is represented by three log-normally distributed modes: the Aitken, accumulation and coarse modes. Each size mode is represented by three moments (3-moment scheme): the total particle number (0th moment), the total particle

Atmos. Chem. Phys. Discuss., doi:10.5194/acp-2015-946, 2016
Manuscript under review for journal Atmos. Chem. Phys.
Published: 23 February 2016

surface area (2π of the 2nd moment), and the total particle mass ($\frac{4}{3}\pi \times \rho_{ss}$ of the 3rd moment; ρ_{ss} = sea salt dry density). The total mass is split into speciated mass fractions, but the total number and surface area emissions are not. The standard deviation and geometric mean diameter (GMD) of each size mode are not fixed but rather are calculated from the moments when necessary. Binkowski and Roselle (2003) and the CMAQ Wiki (http://www.airqualitymodeling.org/cmaqwiki) describe the CMAQ aerosol mechanism in greater detail.

2.2 Sea Salt Emissions

In this section, sea salt emissions are described from three perspectives: (1) the physical processes related to sea salt emissions, (2) the sea salt emission parameterizations compared in this study, and (3) the technical implementation of the sea salt emission parameterizations for CMAQ.

2.2.1 Physical Processes

Water droplets are emitted from the sea surface by the bursting of bubbles (film and jet droplets), by the breaking of waves (splash droplets) and by high wind speeds (spume droplets). The droplet water evaporates until the droplet water content is in equilibrium with the ambient relative humidity. This droplet is denoted as wet sea salt particles.

When air is mixed into sea water by processes such as the breaking of waves, the air forms bubbles, which then rise to the sea surface where they burst. Small water droplets are ejected from the breaking hull of a bubble (film droplets). Because of the abrupt change in pressure within the bursting bubble, water is also sucked from below the bubble into the air (jet droplets). The bursting of bubbles is the most relevant process for sea salt particle production. An increase in wind speed increases wave generation, wave breaking, and, consequently, bubble-bursting-generated sea salt emissions. Sea salt particles from spume and splash droplets are very large and commonly fall back into the ocean within a short time after their emission. They are only relevant at high wind speeds (Lewis and Schwartz, 2004). The SST affects the formation and bursting of air bubbles (Martensson et al., 2003; Callaghan et al., 2014; Grythe et al., 2014), thereby altering the size distribution of the sea salt particles thus produced. Changing the SAL also alters the particle size - a lower salinity leads to smaller particles (Martensson et al., 2003). Moreover, organic species are relevant to sea salt emissions, but their actual impact has not yet been well quantified.

In the surf zone, which is the region along a coast line where waves break, sea salt emissions are enhanced because of the higher number of breaking waves in this relatively small region. Addressing surf zone emissions is quite difficult because they depend on the direction of the waves, the direction of the wind, and local coastal features such as steep cliff coasts and flat beaches.

2.2.2 Sea Salt Emission Parameterizations

The existing sea salt emission parameterizations and their historical development have been extensively described and compared in Lewis and Schwartz (2004), O'Dowd and de Leeuw (2007), de Leeuw et al. (2011), Tsyro et al. (2011), and Spada et al. (2013).

Atmos. Chem. Phys. Discuss., doi:10.5194/acp-2015-946, 2016
Manuscript under review for journal Atmos. Chem. Phys.
Published: 23 February 2016

Atmospheric Chemistry and Physics Discussions

Table 1. Overview of sea salt emission parameterizations GO03, SP13, and OV14.

Parameter-ization	Functional Relation	Wind Dependence	Surf Zone	Parameters	Range of Validity	Reference
GO03	two log-normal distributions	MO80	KE10	u_{10}, SAL[a]	$0.07\ \mu m \leq D_{dry} \leq 20\ \mu m$	Gong (2003)
SP13	mixed	mixed	mixed	u_{10}, SST, SAL[a]	$0.02\ \mu m \leq D_{dry} \leq 30\ \mu m$	Spada et al. (2013)
MA03	three polynomials	MO80	KE10	u_{10}, SST, SAL[a]	$0.02\ \mu m \leq D_{dry} \leq 2.8\ \mu m$	Martensson et al. (2003)
MO86	special function	MO80	KE10	u_{10}, SAL[a]	$2.8\ \mu m \leq D_{dry} \leq 8\ \mu m$ [b]	Monahan et al. (1986)
SM93	two log-normal distributions	own: wind	no	u_{10}, SAL[a]	$2.8\ \mu m \leq D_{dry} \leq 30\ \mu m$ and $u_{10} \geq 9\ m\ s^{-1}$	Smith et al. (1993)
OV14	five log-normal distributions	own: wind and waves	no	u_{10}, H_S, u_* SAL, SST	$0.015\ \mu m \leq D_{dry} \leq 6\ \mu m$ $Re_{Hw} \geq 10^5$ [c]	Ovadnevaite et al. (2014)

[a] Originally, the parameterization does not depend on the SAL. The SAL dependence was added in this study. [b] MO86 is valid on the size range $2.8\ \mu m \leq D_{dry} \leq 8\ \mu m$ if it is not used in this context. [c] The fifth mode is only valid for $Re_{Hw} \geq 2 \times 10^5$.
Abbreviations: MO80 refers to Monahan and Muircheartaigh (1980), KE10 refers to Kelly et al. (2010), $u_{10} = 10$ m wind speed, SAL = sea surface salinity, SST = sea surface temperature, H_S = significant wave height, u_* = friction velocity at sea surface, D_{dry} = dry sea salt particle diameter.

Three parameterizations, developed by Gong (2003), Spada et al. (2013), and Ovadnevaite et al. (2014), and a reference case without any sea salt emissions are compared in this study. They are abbreviated as GO03, SP13, OV14, and zero, respectively. GO03 is the standard parameterization in CMAQ (Kelly et al., 2010). SP13 consists of three existing parameterizations proposed by Martensson et al. (2003) (MA03), Monahan et al. (1986) (MO86), and Smith et al. (1993) (SM93). Table 1 presents an overview of these parameterizations. Relevant aspects thereof are described below. The formulas are provided in the appendix (Eq. (B1) to (B7)). A more detailed description of the formulas and of their implementation are provided in the supplement to this paper (Sect. S1).

All three parameterizations describe the size distribution of sea salt particle emissions in terms of number. For their implementation in CMAQ, log-normal distributions are preferred. GO03 represented by two log-normal distributions, in CMAQ, and describes the bubble-generated production of sea salt particles. SP13 consists of a combination of different types of functions and cannot be simply represented using log-normal distributions. It describes the production of sea salt particles generated by bursting bubbles (MA03 and MO86) and spume droplets (SM93). Spume droplet production is activated at wind speeds above 9 m/s (Monahan et al., 1986). MA03 is based on laboratory studies. Finally, OV14 is a linear combination of five log-normal distributions. It describes bubble-bursting- and spume-droplet-generated sea salt emissions and is based on measurements recorded at Mace Head, Ireland.

The wind speed dependence of GO03 and SP13 (MA03 and MO86) is described by the whitecap coverage parameterization proposed by Monahan and Muircheartaigh (1980). It relates the 10 m wind speed, u_{10} $\left[\mathrm{m\ s^{-1}}\right]$, to the fraction of the sea

Atmos. Chem. Phys. Discuss., doi:10.5194/acp-2015-946, 2016
Manuscript under review for journal Atmos. Chem. Phys.
Published: 23 February 2016

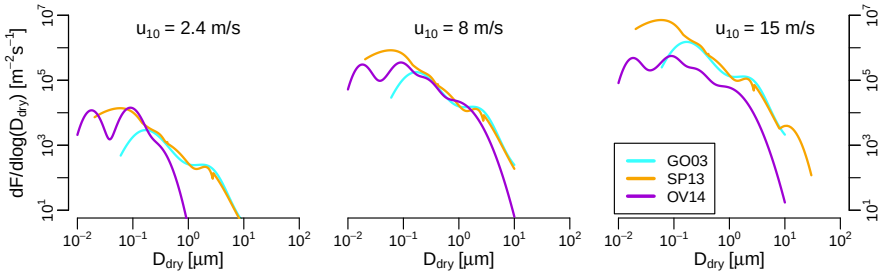

Figure 2. Comparison of the source functions and their wind speed dependence. The largest size mode of OV14 is deactivated for $Re_{Hw} \leq 2 \times 10^5$, and all modes are deactivated for $Re_{Hw} \leq 10^5$ (see Eq. (B7) for the definition of $\mathrm{Re_{Hw}}$). In SP13, a spume-droplet-generated mode represented by SM93 is activated for $u_{10} \geq 9m/s$. The parameters used were as follows: SST = 283 K, SAL = 35‰, $C_D = 2.15 \times 10^{-3}$, $H_S = 1.23$ m, and $\nu_w = 1.34 \times 10 - 6m2/s$

surface covered by whitecaps, denoted by the whitecap coverage W. Bubble bursting and, consequently, sea salt production depend linearly on the whitecap coverage. W (Eq. (1)) scales the distribution functions but does not alter their shape. OV14 employs another wind speed dependence. Each of the five modes is scaled by an individual power-law function depending on a Reynolds number, $\mathrm{Re_{Hw}}$, which is calculated from the friction velocity at the sea surface, u_* $\left[\mathrm{m\ s^{-1}}\right]$; the significant wave height, H_S $[\mathrm{m}]$; and the sea water kinetic viscosity, ν_w $\left[\mathrm{m^2\ s^{-1}}\right]$. The parameter u_* is calculated from u_{10} and a wave drag coefficient, C_D. The parameter ν_w depends on the SST and SAL and is calculated in accordance with Eqs. (8) and (22) in Sharqawy et al. (2010).

$$W = 3.84 \times 10^{-6} \times u_{10}^{3.41} \tag{1}$$

In the surf zone, the sea salt particle number flux is considerably enhanced compared with that in the open ocean. Kelly et al. (2010) proposed the approach to addressing surf zone emissions that is used in CMAQ, namely, the whitecap coverage W is set to 1 in the surf zone which is assumed to have a width of 50 m. CMAQ simulations of parts of Florida performed well with this definition of the surf zone (Kelly, 2014).

2.2.3 Technical Implementation

The aerosol particles in CMAQ are represented by particle number, surface area, and mass concentrations (see Sect. 2.1). Therefore, the total particle number, surface area, and mass emissions per size mode must be provided in CMAQ. However, non-sea-salt-particle emissions are read in only as total mass emissions via external input files. These mass emissions are split into the three size modes using pre-defined splitting factors. The number and surface area emissions are calculated on the basis of standardized geometric mean diameters (GMD) and standard deviations for each mode. By contrast, for sea salt emissions in the standard CMAQ setup, all three values are calculated online in the sea salt emission module based on Gong (2003). The parameterization is fitted to two log-normal distributions (Fig. 3), with the GMD, the standard deviation, and the 0th and 3rd moments being prescribed in the sea salt emission module of CMAQ. The number, surface area, and mass emissions

Atmos. Chem. Phys. Discuss., doi:10.5194/acp-2015-946, 2016
Manuscript under review for journal Atmos. Chem. Phys.
Published: 23 February 2016

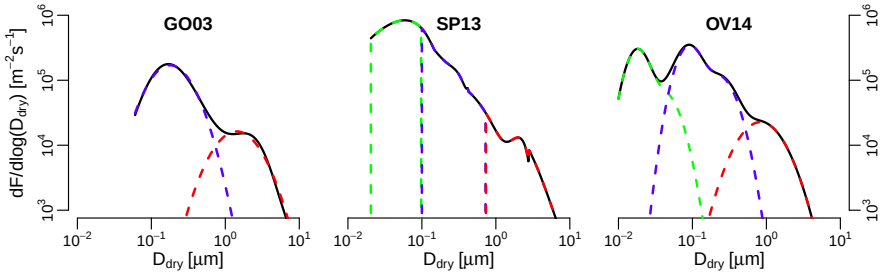

Figure 3. Modal splitting of the sea salt emission parameterizations GO03 (left), SP13 (center), and OV14 (right). The color indicates the size mode in which the sea salt is emitted: green corresponds to the Aitken mode, blue to the accumulation mode and red to the coarse mode.

are calculated from these prescribed parameters. One of the distributions represents the accumulation mode, and the other represents the coarse mode. For the GO03 emission case, this portion of the implementation was left unchanged. By contrast, the SP13 and OV14 emissions (number, surface area, and mass) were calculated externally and read by CMAQ at run time.

Because OV14 consists of five log-normally distributed modes, the two finest size modes were assigned to the Aitken mode in CMAQ, the third and fourth finest size modes were assigned to the accumulation mode, and the largest size mode was assigned to the coarse mode. Because SP13 is not based on log-normally distributed modes, it was integrated within fixed boundaries to split it into the Aitken, accumulation, and coarse modes. The boundary between the Aitken and accumulation modes was set to $D_{\mathrm{dry}} = 0.1\ \mu\mathrm{m}$, and the boundary between the accumulation and coarse modes was set to the intersection between the accumulation and coarse modes for GO03 ($D_{\mathrm{dry}} \approx 1.5\ \mu\mathrm{m}$), which depends somewhat on the relative humidity (see Sect. S4.1 in the supplement).

The SAL in the Baltic Sea is very low - below 10‰ throughout large regions - which requires the inclusion of an SAL dependence in the sea salt emission calculation. For GO03, the approach described in Neumann et al. (2015) was applied: number, surface area, and mass emissions were multiplied by $\frac{\mathrm{SAL}}{35‰}$. OV14 already includes salinity as a parameter. For SP13, we added an SAL dependence based on plots published by Martensson et al. (2003): the size of the emitted sea salt particles was scaled by $\left(\frac{\mathrm{SAL}}{35‰}\right)^{1/3}$. Graphically, the number emission distribution (Fig. 3 center and Fig. 2 orange line) shifts to the left as the SAL decreases (Fig. S1). The Aitken/accumulation and accumulation/coarse mode integration boundaries were held constant, leading to a decrease in the coarse-mode number emissions with a decreasing SAL. Detailed information on the salinity dependence is provided in the supplement (Sect. S3). The surf zone is treated differently in the three parameterizations. In CMAQ (GO03), the surf zone is treated in accordance with Kelly et al. (2010) by setting the whitecap coverage W is set to 1 in the surf zone. In this study, calculations of the surf zone size were performed for a $50\ \mathrm{m}$ wide surf zone by ArcGIS avoiding double-counting of overlapping surf zone stripes (Neumann et al., 2015). The procedure of setting W to 1 can also be applied for SP13 because MA03 and MO86 depend on the same whitecap coverage parameterization as does GO03 (see Sect. S2). However, the SM93 coarse emissions remain unchanged. This approach cannot be applied to OV14 without modification because the wind speed dependence of OV14 is not based on the whitecap coverage approach. Therefore, no surf zone treatment for OV14 was introduced. The total emitted sea salt mass was split into 7.6% $\mathrm{SO_4^{2-}}$, 53.9% $\mathrm{Cl^-}$, and 38.6% $\mathrm{Na^+}$ (Kelly et al.,

Atmos. Chem. Phys. Discuss., doi:10.5194/acp-2015-946, 2016
Manuscript under review for journal Atmos. Chem. Phys.
Published: 23 February 2016

Atmospheric Chemistry and Physics Discussions

2010). The Na^+ in the model includes Na^+, Mg^{2+}, K^+, and Ca^{2+}; only 78% of the Na^+ in the model is true Na^+. This split was applied for all three parameterizations. In addition to dry sea salt, water is also emitted. For GO03, the water content was calculated according to Zhang et al. (2005), and for SP13 and OV14, it was calculated according to Lewis and Schwartz (2006). Both relations are based on data from Tang et al. (1997). The new sea salt emissions were calculated externally and read at run time by CMAQ. The CMAQ sea salt emission module (SSEMIS.F) was modified for this purpose. In the modified version, sea salt emissions can be calculated internally or read in from an external source. Currently, no Aitken-mode sea salt particles are considered in standard CMAQ. The sea salt emission and aerosol emission modules (AERO_EMIS.F) were modified to consider Aitken-mode sea salt emissions in addition to those considered in the standard implementation. The modified CMAQ modules are attached as supplementary material and briefly documented in Sect. S6.

2.3 Geophysical Input and Emission Data

The land-based emissions were compiled by SMOKE for Europe (Bieser et al., 2011) with the agricultural emissions in accordance with Backes et al. (2015a, b). Dust emissions were not included. Shipping emissions were calculated bottom up using ship movement and ship characteristics data (Aulinger et al., 2015).

The meteorological input data were generated by COSMO-CLM (Consortium for Small-scale Modeling in Climate Mode) (Geyer and Rockel, 2013; Geyer, 2014). The used data set is part of the coastDatII database of the Helmholtz-Zentrum Geesthacht (Weisse et al., 2015) (http://www.coastdat.de/). The coastDatII database also contains modeled data for wave and ocean currents, which are forced by COSMO-CLM meteorology. The model grid spans the entire model domain. The data were remapped onto the CMAQ grid, and relevant variables were extracted and converted using a modified version of CMAQ's Meteorology-Chemistry Interface Processor (MCIP) (Otte and Pleim, 2010).

Wave data (H_S and u_*), SAL values, and SST values are required for calculating the new sea salt emissions. For the North Sea, H_S and u_* were obtained from the coastDatII database modeled by the Wave Model (WAM) (Groll et al., 2014). However, Baltic Sea wave data were not available from this database. The significant wave height data for the other seas were acquired from the ERA-Interim wave data set, which was calculated by WAM for a global domain (Dee et al., 2011). No friction velocity data, u_*, were available from that data set; hence, the values of this quantity were calculated from u_{10} (Wu, 1982) using Eqs. (S12) and (S13).

No SAL and SST fields are present in coastDatII. For the North and Baltic Seas, these data were acquired from operational model runs of the German Federal Maritime and Hydrographic Agency (Bundesamt f$\breve{}$r Seeschifffahrt und Hydrographie, BSH) at two different resolutions (see Fig. S2) produced by their model BSHcmod. For the other seas, ERA-Interim SST data were used. The SAL was set to 35‰ in the Atlantic Ocean, 37‰ in the Mediterranean Sea, and 18‰ in the Black Sea.

A detailed listing of the input data sets (Table S6) and their spatial extend (Fig. S2) are given in the supplement (Sect. S5).

2.4 Model Evaluation

The modeled sodium concentrations were compared with the sodium concentrations measured at 11 EMEP stations. The EMEP data (Tørseth et al., 2012) were obtained from the EBAS database (http://ebas.nilu.no/). The sodium concentration is

Atmos. Chem. Phys. Discuss., doi:10.5194/acp-2015-946, 2016
Manuscript under review for journal Atmos. Chem. Phys.
Published: 23 February 2016

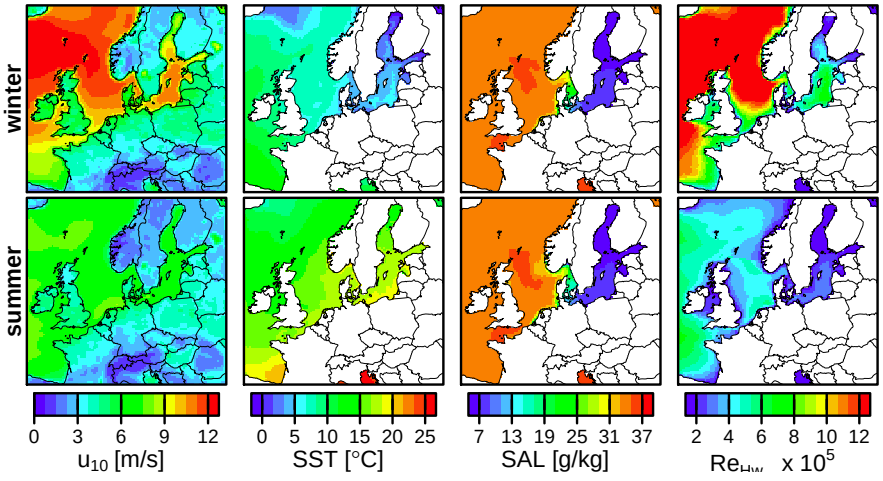

Figure 4. Two-month average u_{10}, SST, SAL, and $\mathrm{Re_{Hw}}$ data are plotted for winter (top) and summer (bottom). $\mathrm{Re_{Hw}}$ was calculated according to Eq. (B7).

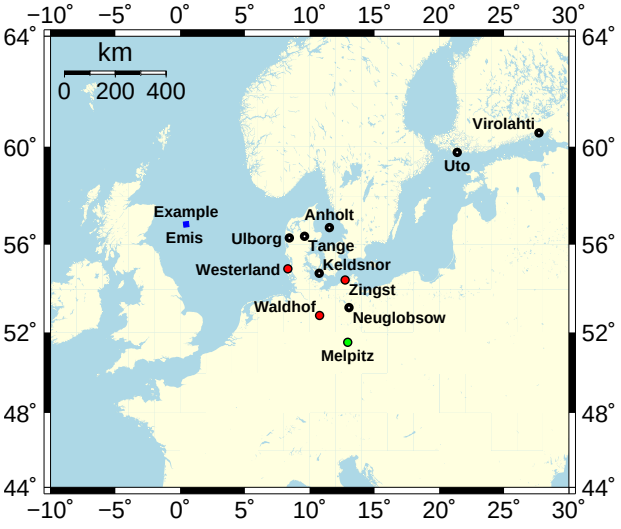

Figure 5. Locations of the EMEP stations at which measured and modeled daily average sodium $\mathrm{PM_{10}}$ data were compared. Red circles: In addition to statistical data being provided, plots are shown and described in detail. Green circle: An additional comparison of $\mathrm{PM_{2.5}}$ data is presented (DE0044R). Blue box: Location of a grid cell which sea salt emissions are presented.

an accurate representation of the sea salt concentration because sea salt is the major source of atmospheric sodium and sodium does not evaporate into the gas phase. Data from winter (January and February) and summer (July and August) of 2008 were considered.

Atmos. Chem. Phys. Discuss., doi:10.5194/acp-2015-946, 2016
Manuscript under review for journal Atmos. Chem. Phys.
Published: 23 February 2016

Atmospheric Chemistry and Physics Discussions

Table 2. EMEP stations that were considered for comparison with the modeled data.

Station ID	Station Name	Data	Lon	Lat	Height [m]	Location
DE0001R	Westerland	PM_{10}	8.31	54.93	12	Coast
DE0002R	Waldhof	PM_{10}	10.76	52.80	74	Inland
DE0007R	Neuglobsow	PM_{10}	13.03	53.17	62	Inland
DE0009R	Zingst	PM_{10}	12.73	54.43	1	Coast
DE0044R	Melpitz	PM_{10}, $PM_{2.5}$	12.93	51.53	86	Inland [a]
DK0003R	Tange	PM_{10}	9.60	56.35	13	Inland
DK0005R	Keldsnor	PM_{10}	10.73	54.73	10	Coast
DK0008R	Anholt	PM_{10}	11.52	56.72	40	Coast
DK0031R	Ulborg	PM_{10}	8.43	56.28	10	Coast
FI0009R	Utö	PM_{10}	21.38	59.78	7	Coast
FI0017R	Virolahti II	PM_{10}	27.69	60.53	4	Coast

[a] located far inland but often influenced by coastal air

The stations considered in the comparison are listed in Table 2 and plotted in Fig. 5. The last column in Table 2 indicates whether each station is located on the coast or inland (more than 50 km distance to the next coast in upwind direction). Daily average PM_{10} measurement data are available at all of the stations. In addition, at Melpitz, $PM_{2.5}$ measurements are available and compared against model data. All stations were compared on the basis of statistical parameters: the residual absolute error (RAE), the mean normalized bias (MNB), and Spearman's correlation coefficient (R). The formulas for the RAE, the MNB, and R are given in the appendix as Eqs. (C1) to (C3), respectively. In addition, the data from the Westerland (DE0001R), Waldhof (DE0002R), Zingst (DE0009R) (PM_{10}, each), and Melpitz (PM_{10} and $PM_{2.5}$) stations were compared graphically.

For the comparison of model and measurement data, PM_{10}, $PM_{2.5}$ and PM_C (= PM_{10} - $PM_{2.5}$) data were extracted from the model simulation results. PM_{10} equals the whole modeled particle mass, $PM_{2.5}$ sums the particle mass of each model mode which is below 2.5 µm, and PM_C is the difference between PM_{10} and $PM_{2.5}$. PM_C does not equal the modeled coarse-mode mass and $PM_{2.5}$ does not equal the sum of Aitken- and accumulation-mode mass.

3 Results and Discussion

The first part of this section offers a review of the sea salt emissions produced by the parameterizations. The second part presents a review of the resulting atmospheric concentrations. Finally, the section closes with a summary.

Atmos. Chem. Phys. Discuss., doi:10.5194/acp-2015-946, 2016
Manuscript under review for journal Atmos. Chem. Phys.
Published: 23 February 2016

Atmospheric Chemistry and Physics Discussions

3.1 Sea Salt Emissions

In this section, sea salt mass (Sect. 3.1.1), surface area (3.1.2), and number emissions (3.1.3) are described and discussed. The particle surface area is the most important of the three parameters because it governs the impact of the sea salt particles on the atmospheric chemistry: a larger surface area yields a stronger condensation of gases onto sea salt. However, this parameter is not measured. By contrast, measurements of the speciated particle mass are standardized and available at several measurement stations. Particle number measurements are more complicated to perform, only available at a few stations and not divided into species but given as bulk number concentration. In order to describe the atmospheric behavior of particle distributions accurately, particle mass, surface area and number data are needed. Therefore, considering all three types of emissions is relevant.

Figure 6 shows plots of dry sea salt mass emissions. Plots a to f show two-month average dry mass sea salt emissions in winter (left column) and summer (right column) produced with GO03 (1st row), SP13 (2nd row), and OV14 (3rd row). Figure 6 g shows box plots of the sea salt mass emissions split into Aitken, accumulation and coarse modes (left to right) at a location in the German Bight (blue square in Fig. 5) that is representative of the open ocean. Figures 7 and 8 are similar but show sea salt surface area and number emissions, respectively. The time series corresponding to the box plots in the three figures are given in the supplement (Sect. S8, Figs. S3 to S5).

3.1.1 Sea Salt Mass Emissions

The SP13 sea salt mass emissions are considerably higher than those produced by GO03 and OV14. The winter emissions are higher than the summer emissions because of higher wind speeds. The sea salt mass emissions in the Baltic Sea region are quite low because of the SAL scaling. In addition, the difference in emissions between the North and Baltic Seas is partly caused by differences in wind speed. SP13 emits the most mass per mode, and OV14, the least (Fig. 6, a-f). In the coarse and accumulation modes, the GO03 mass emissions lie between those of SP13 and OV14 but closer to the SP13 emissions. The SP13 mass emissions strongly decrease from winter to summer. As indicated in Fig. 2, an additional coarse particle mode exists in SP13 for high wind speeds ($u_{10} > 9\ \mathrm{m\ s^{-1}}$). The strong decrease in the SP13 mass emissions in summer originates from a reduced production of spume droplets due to fewer occurrences of threshold exceedance by the wind speed. The coarse-mode mass emissions are considerably higher than those in the accumulation and Aitken modes. Therefore, they dominate the mass emissions depicted in Fig. 6 g.

3.1.2 Sea Salt Surface Area Emissions

In Fig. 7 a-f, the SP13 dry sea salt particle surface area emissions exceed the GO03 and OV14 emissions. However, the GO03 and OV14 surface area emissions are higher than their mass emissions in relation to the respective SP13 emissions. The surface area emissions are not relevant for the comparisons presented in this study because no measurement data are available. However, they are relevant when considering condensation processes and the formation of $\mathrm{NO_3^-}$, $\mathrm{NH_4^+}$ and $\mathrm{SO_4^{2-}}$. According to Fig. 7 g, the coarse-mode surface area emissions of GO03 and SP13 are similar to each other, but those of SP13 are slightly

Atmos. Chem. Phys. Discuss., doi:10.5194/acp-2015-946, 2016
Manuscript under review for journal Atmos. Chem. Phys.
Published: 23 February 2016

Atmospheric Chemistry and Physics Discussions

higher. The SP13 accumulation-mode emissions are approximately twice as high as the corresponding GO03 emissions. For all three parameterizations, OV14 produces the lowest emissions in all three modes. The coarse-mode emissions are four to five times as high as the accumulation-mode emissions and ten to fifty times as high as the Aitken-mode emissions. Hence, the coarse-mode surface area emissions represent the greatest contribution to the total surface area emissions shown in plots a - f.

3.1.3 Sea Salt Number Emissions

The highest total number emissions are calculated using SP13. This is because of the large number of ultra-fine particles on the far left of the distribution in the emission parameterization ($D_{\mathrm{dry}} < 0.1\ \mu\mathrm{m}$), as shown in Fig. 2. For the SP13 parameterization, the relative difference between the Baltic Sea and North Sea number emissions is lower than between the Baltic Sea and North Sea mass emissions. This is because the total mass emissions are scaled by SAL/35‰ and the total number emissions are scaled by 1. Investigation of the modal emissions reveals that the highest coarse-mode number emissions are produced by the OV14 parameterization, followed by GO03. In the accumulation mode, the SP13 number emissions are higher than the corresponding GO03 and OV14 emissions. In the Aitken mode, the SP13 emissions are considerably higher than the respective OV14 emissions. The total number emissions are dominated by the Aitken and accumulation modes. Therefore, SP13 produces the highest total sea salt number emissions and GO03 the least highest. GO03 would probably yield considerably higher particle numbers than OV14 if GO03 included Aitken mode particles. Because OV14 produces the highest coarse-mode number emissions, one might assume that it also produces the highest coarse-mode surface area and mass emissions. The reason why this is not the case is because the OV14 coarse mode (Fig. 3) consists of particles with a smaller diameter than those in the other two source functions, as confirmed by the GMD (Fig. S5).

3.2 Sea Salt Concentrations

3.2.1 PM10 Concentrations

The modeled daily average sodium PM_{10} concentrations were compared with the concentrations measured at 11 EMEP stations. Figure 9 shows the sodium concentrations at three German EMEP stations (Westerland, Waldhof and Zingst) in winter and summer. Table 3 reports the corresponding statistical data for all 11 stations. These stations include both coastal and inland stations (see Table 2), whereas the Melpitz station is located far inland.

At Westerland and Zingst (coastal stations), the SP13 case considerably overestimates the Na^+ concentrations and the OV14 case underestimates them. The winter baseline concentrations at Zingst are somewhat well reproduced by all three parameterizations, whereas the highest values (peaks) are not. GO03 overestimates the peak concentrations at Westerland and Zingst. The correlation coefficients for all three parameterizations are similar to each other at both stations and in both seasons. However, the MNB is closest to 0 for the OV14 case, followed by GO03 and then SP13. The MNB of OV14 is usually negative, whereas it is positive for the other two cases. The RAE is highest for SP13, and the RAEs of GO03 and OV14 are similar. For all coastal stations in Table 3, the correlation coefficient decreases from winter to summer, whereas the MNBs and RAEs improve. For Westerland and Zingst, the MNBs and RAEs are highest for SP13. At most coastal stations, the MNBs for the SP13 and

Atmos. Chem. Phys. Discuss., doi:10.5194/acp-2015-946, 2016
Manuscript under review for journal Atmos. Chem. Phys.
Published: 23 February 2016

GO03 cases are positive and those for the OV14 case are negative. It can be concluded that SP13 and GO03 overestimate the sea salt concentrations at coastal stations, whereas OV14 underestimates them. Based on the MNB and RAE, GO03 and OV14 produce more accurate sodium concentrations than does SP13. The correlation coefficients are quite similar to each other and do not indicate a clear ranking. Notably, at Keldsnor (DK0005R), the correlation coefficients are particularly low.

At Waldhof, which is located approximately 200 km inland, the modeled concentrations are more similar to each other than at the other stations. In winter, SP13 and GO03 overestimate several peak concentrations but the baseline concentrations are well reproduced by all three parameterizations. In summer, GO03 underestimates the baseline concentration and SP13 appears to yield the best reproduction of the observations. Inland stations exhibit high correlation coefficients of between 0.6 and 0.8. The SP13 emissions yield the highest correlation coefficients. However, the difference to the correlation coefficients of the GO03 and OV14 cases is small. The inland MNBs of the GO03 and SP13 cases are smaller than those at the coastal stations, indicating less overestimation of the sodium concentrations at inland stations. For the OV14 case, the MNB is positive in approximately half of the inland cases - particularly during winter - whereas it is typically negative at all coastal stations. Thus, OV14 produces fewer underestimations at inland stations. The RAE is often below 0.5 at inland stations, with the exception of Tange (DK0003R). Commonly, the winter MNB and RAE values are higher than those in summer. The MNBs and RAEs for Tange deviate most strongly from those for the other stations in this group. Tange is the station that is located closest to the coast. At Melpitz, the MNB of OV14 is positive in both winter and summer. In winter, the MNBs of SP13 and GO03 at Melpitz are lower than those at the other stations.

The sodium concentrations at coastal stations, such as Westerland and Zingst, are highest for the SP13 emissions and lowest for the OV14 emissions. For locations farther inland, the SP13 and GO03 concentrations decrease more rapidly than the OV14 concentrations, as indicated by the MNBs. At the far-inland station of Melpitz, the SP13 and OV14 cases yield similar sodium concentrations (MNBs, Table 3) that are higher than the GO03 concentrations. In a similar study, Tsyro et al. (2011) also reported slight overestimations at coastal stations and underestimations at inland stations for GO03 sea salt emissions. This indicates that the particle dry deposition velocities for the SP13 and GO03 emission cases are higher than those for OV14 emission case. The different size distributions of the three parameterizations, which are probably responsible for this effect, are described in Sect. 3.2.2.

At the coastal station of Keldsnor (DK0005R), the correlation coefficients are very low. During winter, the RAEs are higher than those at the other stations. The RAEs during summer and the MNBs are in the same range as those at the other stations. Thus, the order of magnitude of the sodium concentrations is well reproduced, but the temporal occurrences of the peak concentrations are not well reproduced with respect to the other stations. Keldsnor is located on an island that is not resolved by the model, as is Anholt (DK0008R). However, Anholt is located on a small island that is surrounded only by water, whereas Keldsnor is located on a larger island in a region of several islands. Therefore, the local wind fields near Keldsnor may not be correctly predicted and consequently, sub-grid deposition processes may not be correctly reproduced by CMAQ, thereby causing the quality of the modeled sea salt concentrations to decline.

Atmos. Chem. Phys. Discuss., doi:10.5194/acp-2015-946, 2016
Manuscript under review for journal Atmos. Chem. Phys.
Published: 23 February 2016

Atmospheric Chemistry and Physics Discussions

3.2.2 Particle Size Distribution

We noted in Sect. 3.2.1 that sodium PM_{10} mass concentrations were overestimated at coastal stations and underestimated at inland stations in the GO03 case, whereas in the OV14 case the concentrations were underestimated at coastal stations and overestimated at inland stations. This behavior was assumed to be caused by different atmospheric particle size distributions in the three emission cases inducing different dry deposition velocities. Therefore, in this section, the sea salt particles size distributions in the GO03, SP13, and OV14 cases and their evolution from their source regions towards inland are analyzed. In addition, we are interested in how well the modeled size distributions represent measurements. This is done by considering the $PM_{2.5}$ and PM_C sodium concentrations (PM_C=PM_{10}−$PM_{2.5}$) and the modeled coarse mode GMDs at the stations Westerland, Waldhof, and Melpitz. Unfortunately, $PM_{2.5}$ measurement data for validating model data were only available at the station Melpitz. The modeled and measured $PM_{2.5}$ and PM_C concentrations from Melpitz are analyzed first (Fig. 10) followed by an evaluation of the modeled PM data at the three stations (Figs. 11 to 13).

For the $PM_{2.5}$ concentrations in summer (Fig. 10, center right), GO03 best reproduces the measured concentrations with respect to their magnitude. SP13 and OV14 yield considerable overestimations. During winter, all parameterizations underestimate the $PM_{2.5}$ peak concentrations, but SP13 overestimates the baseline concentrations, and positive MNBs indicate overestimations in all three cases. The average concentrations are best predicted by OV14, but the MNB is lowest for GO03. The correlation coefficient for OV14 is lower than those for GO03 and SP13 (Table 4). Thus, GO03 produces the best sodium $PM_{2.5}$ predictions, followed by OV14. Because OV14 is based on a highly detailed particle size distribution data set and considers ultra-fine particles (the Aitken mode), it might be expected that this parameterization would yield the best predictions of the $PM_{2.5}$ particle concentrations.

The temporal occurrences of peak PM_C concentrations are not consistently predicted by the three parameterizations, i.e., GO03 and SP13 predict several peaks that are not predicted by OV14, and OV14 also predicts peaks that are not predicted by the other two models. The PM_C concentrations are underestimated by GO03 in summer (MNB = -0.4), which leads to underestimation of the PM_{10} concentrations. In summer, OV14 and SP13 slightly underestimate the coarse particles but moderately overestimate the PM_{10} concentrations because of a considerable overestimation of $PM_{2.5}$. In particular, OV14 considerably overestimates the PM_C concentrations in late August for approximately a week, whereas the other parameterizations predict lower and more accurate concentrations. If this period were to be neglected, a more pronounced negative MNB for OV14 during summer would result. In winter, the coarse particles are overestimated by all parameterizations (MNB > 0); this overestimation is lowest for OV14 and highest for SP13. The correlation coefficients and RAEs for each season are quite similar to each other and provide no clear indication of which parameterization yields better results. Thus, based on the R values and the RAEs, no parameterization produces a clearly superior prediction of PM_C concentrations. However, according to the MNBs, OV14 produces the best results when winter and summer are considered together.

In summary, GO03 produces the best $PM_{2.5}$ concentrations, and OV14 produces the best PM_C concentrations at Melpitz. This size-resolved comparison indicates that PM_{10} concentrations are not necessarily appropriate for validating sea salt emis-

Atmos. Chem. Phys. Discuss., doi:10.5194/acp-2015-946, 2016
Manuscript under review for journal Atmos. Chem. Phys.
Published: 23 February 2016

Atmospheric Chemistry and Physics Discussions

sion parameterizations but that size-resolved measurements are of considerable importance in the validation process. Therefore, size-resolved sodium measurements in coastal regions will be necessary for the further evaluation of sea salt source functions.

For evaluating the evolution of the sodium size distributions, Figs. 11 and 12 depict similar data than Fig. 10 but at the stations Westerland and Waldhof, respectively. Figure 13 shows the modeled coarse-mode GMDs for all particles at Westerland, Waldhof and Melpitz.

At Westerland, PM_C sodium represents the predominant contribution to the total sodium mass in all three sea salt emission parameterizations (Fig. 11). The $PM_{2.5}$ and PM_C concentrations are twice as high during winter than summer. Similar as for the PM_{10} concentrations described above, the SP13 case yields the highest PM_C concentrations and OV14, the least. By contrast, the OV14 case yields higher $PM_{2.5}$ concentrations than the GO03 case in summer. In winter, the $PM_{2.5}$ concentrations of both cases are on the same level. At the station Waldhof (Fig. 12), the $PM_{2.5}$ concentrations are lower compared with the concentrations at Westerland but the ratio between the concentrations in the three cases is similar. By contrast, the PM_C concentrations in the three cases are closer to each other compared with Westerland. In particular, PM_C concentrations produced by OV14 are nearly as high as those produced by GO03. Additionally, the PM_C concentrations decrease stronger from Westerland to Waldhof than the $PM_{2.5}$ concentrations.

At Melpitz, the GO03 and OV14 cases yield quite similar PM_C concentrations. The PM_C concentrations are lower than at Waldhof and considerable lower than at Westerland, particularly the PM_C concentrations in the SP13 and GO03 cases. The decrease of the $PM_{2.5}$ concentrations from Westerland via Waldhof to Melpitz is lower compared to the decrease of PM_C. Consequently, $PM_{2.5}$ and PM_C concentrations are on a similar level at the station Melpitz. Therefore, the relevance of the $PM_{2.5}$ fraction increases with distance to the marine sea salt emission regions. Additionally, this analysis reveals that the deposition of coarse sea salt particles above 2.5 µm diameter is the predominant fraction of the total sea salt mass deposition. Thus, $PM_{2.5}$ sea salt is more relevant for the transport of attached species, which are condensed on the sea salt particle surface, over long distances than PM_C sea salt. The deposition of PM_C mass exhibits to be higher in the SP13 and GO03 cases than in the OV14 case. Therefore, sea salt emission parameterizations including more fine particles as OV14 can be expected to transport higher concentrations of those species over long distances than parameterizations as SP13 that yield a strong dry deposition close to source regions do. In order to understand why PM_C deposition velocities differ in the three emission cases, the GMDs of the modeled coarse mode are considered (Fig. 13). The GMD in the zero case represents the modeled GMD in the absence of sea salt emissions.

The sea salt particle emissions predicted in the SP13 and GO03 cases are larger in terms of the GMD than are those predicted in the OV14 case (Fig. S5). Hence at the stations Westerland, SP13 yields the highest coarse-mode GMDs, followed by GO03 and then OV14 and zero. By contrast, at Waldhof, the GMDs for the different parameterizations are more similar to each other. On average, SP13 produces the highest GMDs, similar to the case of coastal stations. In summer, GMDs in the OV14 case exceed those in the GO03 case. At Melpitz, the GMDs are even closer to each other, whereby the GMDs in the GO03 case decrease below the GMDs in the zero case in some situations. The dry deposition behavior is dependent on particle size; therefore, coarse mass is deposited more rapidly in the SP13 and GO03 cases than in the OV14 case on the journey from the coast via Melpitz to Waldhof.

Atmos. Chem. Phys. Discuss., doi:10.5194/acp-2015-946, 2016
Manuscript under review for journal Atmos. Chem. Phys.
Published: 23 February 2016

Atmospheric Chemistry and Physics Discussions

3.3 General Discussion

In this section, the shortcomings of and possible improvements to the individual sea salt emission parameterizations are discussed. The last paragraph contains technical remarks on the sea salt emission calculations.

Because the SP13 sea salt mass concentrations often considerably exceed the measured sea salt concentrations, it can be assumed that the SP13 emissions are too high. SP13 is based on a laboratory study (Martensson et al., 2003) in which SST-dependent sea salt emissions were measured directly after formation. The particle flux measured in Martensson et al. (2003) was the gross particle flux, which is not necessarily equal to the net particle flux because some particles fall back into the ocean shortly after their emission. This may explain why SP13 overestimates sea salt emissions. The gross emission flux distribution of Martensson might need to be corrected by a size-dependent scaling function to accurately represent the net particle flux. The development of such a scaling function is beyond the scope of this study. Alternatively, the spume droplet production contributed by SM93, which is activated for wind speeds above a threshold of 9 m/s, might be too high. This criterion is exceeded more frequently during winter than summer. This might yield the higher overestimations at coastal stations during winter compared with those during summer, which were noticed in Sect. 3.2.

The elevated overestimation at coastal stations during winter has also been observed in the GO03 case. Because both parameterizations depend on the same whitecap coverage parameterization (Monahan and Muircheartaigh, 1980), the increased overestimation during winter might originate from this whitecap coverage parameterization. Massel (2007b) discussed the sensitivity of the exponent in the whitecap coverage parameterization (Eq. (1)). A lower exponent would reduce the gradient of $W(u_{10})$ and the overestimation at high wind speeds. Additionally, GO03 does not include an SST dependence. As described by Martensson et al. (2003), Callaghan et al. (2014), and Salter et al. (2015), sea salt emissions decrease with decreasing SST. Thus, an emission reduction in winter due to a low SST might be missing from this model. Using CMAQ version 5.1, different modifications of the GO03 parameterization were compared. Among others, an SST scaling of GO03 emissions published by Jaeglé et al. (2011) was tested and found to improve the modeled sodium concentrations. Therefore, it is unclear whether the classical whitecap coverage dependence or deficiencies in the wind-independent part of the parameterization are responsible for the greater overestimation observed during winter.

In contrast to the GO03 and SP13 emission cases, the OV14 case yielded underestimations of the sodium PM_{10} concentrations at coastal stations. OV14 was fitted to data from the Northeastern Atlantic Ocean and to measurements from Mace Head, Ireland. The Atlantic Ocean is a deep and open ocean, in contrast to the North Sea, which is constrained by several coasts and is quite shallow in most areas. This allows waves to evolve differently; for example, the significant wave height is reduced near Dogger Bank. Hence, it might be necessary to refit the OV14 parameterization to the wave regime in the North Sea, e.g., by scaling $\mathrm{Re}_{\mathrm{Hw}}$ with the wave period or wave length. An alternative approach that utilizes wave data is based on the energy dissipation caused by wave breaking, as reported by Long et al. (2011). These authors related the volume of air entrained into the water via wave breaking to the dissipated energy. The volume of entrained air is considered to be proportional to the number of bursting bubbles and the number of sea salt particles produced. Salter et al. (2015) also employed this approach. However, Long et al. (2011) calculated the dissipated energy from u_{10} using a power-law relation, which is simply another fit similar to

Atmos. Chem. Phys. Discuss., doi:10.5194/acp-2015-946, 2016
Manuscript under review for journal Atmos. Chem. Phys.
Published: 23 February 2016

Atmospheric Chemistry and Physics Discussions

(Eq. (1)) and does not solve the problem of breaking waves in shallow water. Wave models can be used to calculate dissipative energy, as well. However, these estimations are rough because no dissipative energy measurements are available for validation purposes (Massel, 2007a).

Surf zone emissions are not the focus of this study. However, they must be briefly discussed because the three compared sea salt emissions parameterizations allow the surf zone to be considered in different ways. The wind speed dependence adopted in GO03 and SP13 is the classical Monahan whitecap coverage parameterization (Monahan and Muircheartaigh, 1980). Therefore, the CMAQ surf zone approach described by Kelly et al. (2010), namely, a $50\ \mathrm{m}$ wide surf zone in which the whitecap coverage is set to 1, was applied for these two parameterizations. However, OV14 does not incorporate the classical Monahan whitecap coverage treatment. Instead, a Reynolds number (Eq. (B7)) is calculated for the sea surface and input into power laws for scaling the five log-normal particle number distributions. Unfortunately, the Reynolds number decreases toward the coast as a result of the decreasing wind speed and decreasing significant wave height (Fig. 4), which leads to reduced OV14 emissions at the coastline. Thus, the OV14 emissions are reduced in the surf zone, in contrast to the increase in surf zone emissions produced by the two other parameterizations. This may be a second reason why OV14 underestimates the sodium mass concentrations at coastal EMEP stations. An alternative approach that is instead based on the dissipative energy by wave breaking would imply enhanced sea salt emissions in the surf zone and would render a special treatment of the surf zone unnecessary.

The splitting of sea salt emissions into the three aerosol modes is a relevant step that affects the CTM calculations. According to Fig. 2, more coarse particles are produced by the SP13 parameterization than by the other two. However, the modal split is different for all three parameterizations (Fig. 3), leading to the emission of smaller but more numerous coarse-mode particles in the OV14 parameterization compared with the others. Consequently, the derived GMD for the OV14 coarse-mode emissions is smaller than those for the SP13 and GO03 coarse-mode emissions (Fig. S5). This affects the modal distribution of the atmospheric particle concentrations (Figs. 10 to 13) as well as atmospheric processes such as dry deposition. Therefore, the technical aspects of the progression from the emission parameterization to the CTM affects the modeled sea salt particle behavior.

4 Conclusions

In a comparison of the sodium concentrations produced by three sea salt source parameterizations, the GO03 and OV14 parameterizations were identified to produce sodium mass concentrations closest to measurements. When comparing the modeled PM_{10} mass concentrations to observations, the correlation coefficients in all three cases are often similar to each other at individual stations and reveal no overall tendency (Table 3). The MNBs and RAEs indicate that the GO03 and OV14 parameterizations reproduce the measured data better than does the SP13 parameterization, which has the highest MNBs and generally overestimates the sodium concentrations. At coastal stations, OV14 underestimates and GO03 overestimates the sodium concentrations, whereas at inland stations, OV14 partially overestimates and GO03 partially underestimates (Fig. 9). This opposite trend between coastal and inland stations is due to the different dry deposition velocities of the parameterizations originating from their different particle size distributions (Fig. 13). Considering $\mathrm{PM}_{2.5}$ and PM_{10} measurements from Melpitz station,

Atmos. Chem. Phys. Discuss., doi:10.5194/acp-2015-946, 2016
Manuscript under review for journal Atmos. Chem. Phys.
Published: 23 February 2016

Atmospheric Chemistry and Physics Discussions

the three parameterizations reproduce the concentrations in these two size classes with varying degrees of success: GO03 best reproduces the $\mathrm{PM}_{2.5}$ mass concentrations, and OV14 best reproduces the PM_{C} mass concentrations. Unfortunately, no further size-resolved data were available, although measurements from closer to the coast would have been more informative. However, these results clearly indicate that size-resolved measurements are necessary for validating sea salt emission parameterizations. Because particles of different sizes have different deposition velocities, the particle distribution can be estimated based on speciated PM_{10} measurements recorded at different distances from the coast. However, this approach requires the CTMs to accurately reproduce the size distributions of the emitted sea salt particles and their dry deposition behavior.

The GO03 and OV14 emissions yielded the most accurate sodium mass concentrations. However, both parameterizations have certain shortcomings, and improvements to them should be considered. Enhancing GO03 by SST dependence, such as Jaeglé et al. (2011) did, might reduce overestimations, particularly during winter. OV14 was fitted based on wave data from the Northeast Atlantic Ocean to sea salt measurement data recorded at Mace Head, Ireland. However, the wave spectrum in the Atlantic Ocean is different from that in the North Sea; on the one hand, it may require a refit of the OV14 parameterization to the wave spectrum in the study region. Additionally, the possibility of enhancing OV14 with an appropriate representation of surf zone emissions should be considered. On the other hand, considering dissipative energy by wave breaking instead of Reynolds number of the sea surface would probably solve the surf zone and wave spectrum issues.

Appendix A: Abbreviations

Table 5 shows the numbers and meaning of all abbreviations and variables used in the manuscript and in the supplement.

Appendix B: Sea Salt Emission Parameterizations

B1 GO03

The sea salt emissions parameterization GO03 published by Gong (2003) is given by Eq. (B1).

$$\begin{aligned}\frac{dF_{\mathrm{GO03}}}{dr_{80}} &= W \times 3.576 \times 10^{5} r_{80}^{-A}\left(1+0.057 \times r_{80}^{3.45}\right) \times 10^{1.607 e^{-B^2}} \\ &= 1.373 \times u_{10}^{3.41} r_{80}^{-A}\left(1+0.057 \times r_{80}^{3.45}\right) \times 10^{1.607 e^{-B^2}} \\ A &= 4.7 \times (1+\Theta \times r_{80})^{-0.017 \times r_{80}^{-1.44}} \\ B &= \left(0.433-\log_{10} r_{80}\right)/0.433 \\ \Theta &= 30\end{aligned} \tag{B1}$$

The parameterization is valid on the size range $0.07\ \mu\mathrm{m} \leq r_{80} \leq 20\ \mu\mathrm{m}$.

Atmos. Chem. Phys. Discuss., doi:10.5194/acp-2015-946, 2016
Manuscript under review for journal Atmos. Chem. Phys.
Published: 23 February 2016

Atmospheric Chemistry and Physics Discussions

B2 SP13

The parameterization SP13 published by Spada et al. (2013) consists of MO86, SM93, and MA03. Below, all three formulas are given in Eqs. (B2), (B3), and (B4), respectively. Equation (B5) defines the combination of all three parameterizations.

$$\begin{aligned}\frac{dF_{\text{MO86}}}{dr_{80}} &= W \times 3.576 \times 10^{5} r_{80}^{-3} 10^{1.19e^{-B^2}} \\ &= 1.373 \times u_{10}^{3.41} r_{80}^{-3} 10^{1.19e^{-B^2}} \\ B &= \left(0.380 - \log_{10} r_{80}\right)/0.650\end{aligned} \tag{B2}$$

The parameterization is valid on the size range $0.8\ \mu\text{m} \leq r_{80} \leq 20\ \mu\text{m}$.

$$\begin{aligned}\frac{dF_{\text{SM93}}}{dr_{80}} &= \sum_{k=1}^{2} \left(A_k\left(u_{10}\right) \times \exp\left(-f_k \left(\ln\left(\frac{r_{80}}{r_{0k}} \right) \right)^2 \right) \right) \\ \log_{10} A_1 &= 0.0676 \times u_{10} + 2.43 \\ \log_{10} A_2 &= 0.959 \times u_{10}^{0.5} - 1.476 \\ r_{01} &= 2.1\ \mu\text{m}; \qquad r_{02} = 9.2\ \mu\text{m} \\ f_1 &= 3.1; \qquad f_2 = 3.3\end{aligned} \tag{B3}$$

Spada et al. (2013) considers the parameterization to be valid on the size range $5\ \mu\text{m} \leq r_{80} \leq 30\ \mu\text{m}$.

$$\begin{aligned}\frac{dF_{\text{MA03}}}{dD_{\text{dry}}} &= W \times (A \times \text{SST} + B) \\ A &= c_4 \times D_{\text{dry}}^4 + c_3 \times D_{\text{dry}}^3 + c_2 \times D_{\text{dry}}^2 + c_1 \times D_{\text{dry}} + c_0 \\ B &= d_4 \times D_{\text{dry}}^4 + d_3 \times D_{\text{dry}}^3 + d_2 \times D_{\text{dry}}^2 + d_1 \times D_{\text{dry}} + d_0\end{aligned} \tag{B4}$$

The parameterization is valid on the size range $0.02\ \mu\text{m} \leq r_{80} \leq 2.8\ \mu\text{m}$.

$$\frac{dF_{\text{SP13}}}{dD_{\text{dry}}} = \begin{cases} \frac{dF_{\text{MA03}}}{dD_{\text{dry}}} & D_{\text{dry}} \leq 2.8\ \mu\text{m} \\ \frac{dF_{\text{MO86}}}{dD_{\text{dry}}} & D_{\text{dry}} > 2.8\ \mu\text{m} \\ & \wedge\ u_{10} < 9\ \text{m s}^{-1} \\ \max\left(\frac{dF_{\text{MO86}}}{dD_{\text{dry}}}, \frac{dF_{\text{SM93}}}{dD_{\text{dry}}} \right) & D_{\text{dry}} > 2.8\ \mu\text{m} \\ & \wedge\ u_{10} \geq 9\ \text{m s}^{-1} \end{cases} \tag{B5}$$

SP13 is valid on the size range $0.02\ \mu\text{m} \leq D_{\text{dry}} \leq 30\ \mu\text{m}$.

Atmos. Chem. Phys. Discuss., doi:10.5194/acp-2015-946, 2016
Manuscript under review for journal Atmos. Chem. Phys.
Published: 23 February 2016

Atmospheric Chemistry and Physics Discussions

B3 OV14

The sea salt emissions parameterization OV14 published by Ovadnevaite et al. (2014) is given by Eq. (B6).

$$\frac{dF_{\mathrm{OV14}}}{d\log_{10} D_{\mathrm{dry}}} = \sum_{i=1}^{5} \frac{F_i\left(\mathrm{Re_{Hw}}\right)}{\sqrt{2\pi} \times \log_{10}\sigma_i} \times \exp\left(-\frac{1}{2}\left(\frac{\log_{10}\frac{D_{\mathrm{dry}}}{\mathrm{GMD}_i}}{\log_{10}\sigma_i}\right)\right) \tag{B6}$$

$$\mathrm{Re_{Hw}} = \frac{u_* \times H_S}{\nu_W} = \frac{\sqrt{C_D} \times u_{10} \times H_S}{\nu_W} \tag{B7}$$

The kinetic viscosity ν_W is calculated according to Eqs. (22) and (8) in Sharqawy et al. (2010). The source function is valid on the size range $0.015\ \mu\mathrm{m} < D_{\mathrm{dry}} < 6\ \mu\mathrm{m}$. The values for GMD_i, σ_i, and F_i are given in the supplement (Table S2) and in Ovadnevaite et al. (2014).

Appendix C: Statistical Evaluation

The statistical figures residual absolute error (RAE), mean normalized bias (MNB), and Spearman's correlation coefficient (R) are calculated according to Eqs. (C1), (C2), and (C3) , respectively.

$$\mathrm{RAE} = \frac{1}{n} \times \sum_{i=1}^{n} |P_i - O_i| \tag{C1}$$

$$\mathrm{MNB} = \frac{1}{n} \times \sum_{i=1}^{n} \frac{P_i - O_i}{O_i} \tag{C2}$$

$$\mathrm{R} = 1 - \frac{6}{n\left(n^2-1\right)} \times \sum_{i=1}^{n} \left(P_i - O_i\right)^2 \tag{C3}$$

with

- P_i i$^{\mathrm{th}}$ predicted value
- p_i rank of the i$^{\mathrm{th}}$ predicted value
- O_i i$^{\mathrm{th}}$ observed value
- o_i rank of the i$^{\mathrm{th}}$ observed value
- n number of observations

Acknowledgements. For the calculation of sea salt emissions, input data were obtained from the European Centre for Medium-Range Weather Forecasts (ECMWF), the German Federal Maritime and Hydrographic Agency (BSH), and the coastDatII database of Helmholtz-Zentrum Geesthacht (HZG). In particular, Beate Geyer and Nikolaus Groll supported this work by preparing the coastDatII meteorological and wave data, respectively, and by answering several questions about these data. We thank Matthias Karl and Jan Arndt for fruitful discussions and literature references as well as Markus Schultze and Joanna Staneva for providing additional information on the meteorological and wave data. Jim Kelly, Brett Gantt and Uma Shankar (U.S. EPA) answered questions about the implementation of the sea salt emission calculations

Atmos. Chem. Phys. Discuss., doi:10.5194/acp-2015-946, 2016
Manuscript under review for journal Atmos. Chem. Phys.
Published: 23 February 2016

Atmospheric Chemistry and Physics Discussions

in CMAQ, and Monica Mårtensson (Uppsala University), Astrid Manders-Groot (TNO) and Jurgita Ovadnevaite (National University of Ireland) provided helpful comments with respect to their sea salt studies and sea salt emission parameterizations. We offer our general gratitude to the U.S. EPA and the CMAQ development team for providing this high-quality chemistry transport model as an open-source product. The EMEP measurement data were extracted from the EBAS database, which is maintained and updated by the Norwegian Institute for Air Research (NILU). In particular, we thank Anne Hjellbrekke for answering questions about the EMEP data. The statistical evaluations and most plotting tasks were performed using R. The remaining plots were created using the Generic Mapping Tools (GMT) developed and maintained by Paul Wessel, Walter H. F. Smith, Remko Scharroo, Joaquim Luis and Florian Wobbe. The simulation data were processed using the Climate Data Operators (CDO) suite developed by Uwe Schultz-Weider from the Max-Planck-Institute for Meteorology and using the netCDF Operators (NCO) suite developed by Charlie Zender and Henry Butowsky. Finally, we thank American Journal Experts (AJE) for English language editing.

Atmos. Chem. Phys. Discuss., doi:10.5194/acp-2015-946, 2016
Manuscript under review for journal Atmos. Chem. Phys.
Published: 23 February 2016

Atmospheric Chemistry and Physics Discussions

References

Aulinger, A., Matthias, V., Zeretzke, M., Bieser, J., Quante, M., and Backes, A.: The impact of shipping emissions on air pollution in the Greater North Sea region - Part 1: Current emissions and concentrations, Atmos. Chem. Phys. Discussions, 15, 11 277–11 323, doi:10.5194/acpd-15-11277-2015, 2015.

Backes, A., Aulinger, A., Bieser, J., Matthias, V., and Quante, M.: Ammonia Emissions In Europe, Part I: Development of a dynamical ammonia emissions inventory, Atmos. Env., under review, 2015a.

Backes, A., Aulinger, A., Bieser, J., Matthias, V., and Quante, M.: Ammonia emissions in Europe, Part II: How ammonia emission abatement strategies affect secondary aerosols, Atmos. Env., under review, 2015b.

Bieser, J., Aulinger, A., Matthias, V., Quante, M., and Builtjes, P.: SMOKE for Europe - adaptation, modification and evaluation of a comprehensive emission model for Europe, Geosci. Model Dev., 4, 47–68, doi:10.5194/gmd-4-47-2011, 2011.

Binkowski, F. S. and Roselle, S. J.: Models-3 Community Multiscale Air Quality (CMAQ) model aerosol component 1. Model description, J. Geophys. Res. Atmos., 108, 4183, doi:10.1029/2001JD001409, 2003.

Blanchard, D. C.: Sea-to-Air Transport of Surface Active Material, Science, 146, 396–397, doi:10.1126/science.146.3642.396, 1964.

Blanchard, D. C. and Woodcock, A. H.: The Production, Concentration, and vertical Distribution of the Sea-Salt Aerosol, Ann. NY. Acad. Sci., 338, 330–347, doi:10.1111/j.1749-6632.1980.tb17130.x, 1980.

Cai, X., Ziemba, L. D., and Griffin, R. J.: Secondary aerosol formation from the oxidation of toluene by chlorine atoms, Atmos. Environ., 42, 7348 – 7359, doi:10.1016/j.atmosenv.2008.07.014, 2008.

Callaghan, A. H., Stokes, M. D., and Deane, G. B.: The effect of water temperature on air entrainment, bubble plumes, and surface foam in a laboratory breaking-wave analog, J. Geophys. Res.-Oceans, 119, 7463–7482, doi:10.1002/2014JC010351, 2014.

Cavalli, F., Facchini, M. C., Decesari, S., Mircea, M., Emblico, L., Fuzzi, S., Ceburnis, D., Yoon, Y. J., O'Dowd, C. D., Putaud, J.-P., and Dell'Acqua, A.: Advances in characterization of size-resolved organic matter in marine aerosol over the North Atlantic, J. Geophys. Res. Atmos., 109, doi:10.1029/2004JD005137, 2004.

Crisp, T. A., Lerner, B. M., Williams, E. J., Quinn, P. K., Bates, T. S., and Bertram, T. H.: Observations of gas phase hydrochloric acid in the polluted marine boundary layer, J. Geophys. Res. Atmos., 119, 6897–6915, doi:10.1002/2013JD020992, 2014.

de Leeuw, G., Andreas, E. L., Anguelova, M. D., Fairall, C. W., Lewis, E. R., O'Dowd, C., Schulz, M., and Schwartz, S. E.: Production flux of sea spray aerosol, Rev. Geophys., 49, n/a–n/a, doi:10.1029/2010RG000349, 2011.

Dee, D. P., Uppala, S. M., Simmons, A. J., Berrisford, P., Poli, P., Kobayashi, S., Andrae, U., Balmaseda, M. A., Balsamo, G., Bauer, P., Bechtold, P., Beljaars, A. C. M., van de Berg, L., Bidlot, J., Bormann, N., Delsol, C., Dragani, R., Fuentes, M., Geer, A. J., Haimberger, L., Healy, S. B., Hersbach, H., Hólm, E. V., Isaksen, L., Kållberg, P., Köhler, M., Matricardi, M., McNally, A. P., Monge-Sanz, B. M., Morcrette, J.-J., Park, B.-K., Peubey, C., de Rosnay, P., Tavolato, C., Thépaut, J.-N., and Vitart, F.: The ERA-Interim reanalysis: configuration and performance of the data assimilation system, Q. J. Roy. Meteor. Soc., 137, 553–597, doi:10.1002/qj.828, 2011.

Donaldson, D. J., , and Vaida, V.: The Influence of Organic Films at the Air - Aqueous Boundary on Atmospheric Processes, Chemical Reviews, 106, 1445–1461, doi:10.1021/cr040367c, pMID: 16608186, 2006.

Fairall, C. W., Davidson, K. L., and Schacher, G. E.: An analysis of the surface production of sea-salt aerosols, Tellus B, 35B, 31–39, doi:10.1111/j.1600-0889.1983.tb00005.x, 1983.

Gantt, B., Kelly, J. T., and Bash, J. O.: Updating sea spray aerosol emissions in the Community Multiscale Air Quality (CMAQ) model version 5.0.2, Geosci. Model Dev., 8, 3733–3746, doi:10.5194/gmd-8-3733-2015, 2015.

Geyer, B.: High-resolution atmospheric reconstruction for Europe 1948-2012: coastDat2, Earth Syst. Sci. Data, 6, 147–164, doi:10.5194/essd-6-147-2014, 2014.

Geyer, B. and Rockel, B.: coastDat-2 COSMO-CLM Atmospheric Reconstruction, World Data Center for Climate (WDCC), Hamburg, Germany, doi:10.1594/WDCC/coastDat-2_COSMO-CLM, 2013.

Gong, S. L.: A parameterization of sea-salt aerosol source function for sub- and super-micron particles, Global Biogeochem. Cycles, 17, 1097, doi:10.1029/2003GB002079, 2003.

Groll, N., Grabemann, I., and Gaslikova, L.: North Sea wave conditions: an analysis of four transient future climate realizations, Ocean Dynam., 64, 1–12, doi:10.1007/s10236-013-0666-5, 2014.

Grythe, H., Ström, J., Krejci, R., Quinn, P., and Stohl, A.: A review of sea-spray aerosol source functions using a large global set of sea salt aerosol concentration measurements, Atmos. Chem. Phys., 14, 1277–1297, doi:10.5194/acp-14-1277-2014, 2014.

Huijnen, V., Williams, J., van Weele, M., van Noije, T., Krol, M., Dentener, F., Segers, A., Houweling, S., Peters, W., de Laat, J., Boersma, F., Bergamaschi, P., van Velthoven, P., Le Sager, P., Eskes, H., Alkemade, F., Scheele, R., Nédélec, P., and Pätz, H.-W.: The global chemistry transport model TM5: description and evaluation of the tropospheric chemistry version 3.0, Geosci. Model Dev., 3, 445–473, doi:10.5194/gmd-3-445-2010, 2010.

Im, U.: Impact of sea-salt emissions on the model performance and aerosol chemical composition and deposition in the East Mediterranean coastal regions, Atmos. Environ., 75, 329 – 340, doi:10.1016/j.atmosenv.2013.04.034, 2013.

Jaeglé, L., Quinn, P. K., Bates, T. S., Alexander, B., and Lin, J.-T.: Global distribution of sea salt aerosols: new constraints from in situ and remote sensing observations, Atmos. Chem. Phys., 11, 3137–3157, doi:10.5194/acp-11-3137-2011, 2011.

Kelly, J. T.: personal communication, 2014.

Kelly, J. T., Bhave, P. V., Nolte, C. G., Shankar, U., and Foley, K. M.: Simulating emission and chemical evolution of coarse sea-salt particles in the Community Multiscale Air Quality (CMAQ) model, Geosci. Model Dev., 3, 257–273, doi:10.5194/gmd-3-257-2010, 2010.

Knipping, E. M. and Dabdub, D.: Impact of Chlorine Emissions from Sea-Salt Aerosol on Coastal Urban Ozone, Environ. Sci. Technol., 37, 275–284, doi:10.1021/es025793z, 2003.

Lewis, E. R. and Schwartz, S. E.: Sea Salt Aerosol Production: Mechanisms, Methods, Measurements and Models - A Critical Review, vol. 152, AGU, Washington, D. C., doi:10.1029/GM152, 2004.

Lewis, E. R. and Schwartz, S. E.: Comment on "size distribution of sea-salt emissions as a function of relative humidity", Atmos. Environ., 40, 588 – 590, doi:10.1016/j.atmosenv.2005.08.043, 2006.

Long, M. S., Keene, W. C., Kieber, D. J., Erickson, D. J., and Maring, H.: A sea-state based source function for size- and composition-resolved marine aerosol production, Atmos. Chem. Phys., 11, 1203–1216, doi:10.5194/acp-11-1203-2011, 2011.

Manders, A., Schaap, M., Querol, X., Albert, M., Vercauteren, J., Kuhlbusch, T., and Hoogerbrugge, R.: Sea salt concentrations across the European continent, Atmos. Environ., 44, 2434 – 2442, doi:10.1016/j.atmosenv.2010.03.028, 2010.

Martensson, E. M., Nilsson, E. D., de Leeuw, G., Cohen, L. H., and Hansson, H.-C.: Laboratory simulations and parameterization of the primary marine aerosol production, J. Geophys. Res. Atmos., 108, 4297, doi:10.1029/2002JD002263, 2003.

Massel, S. R.: Ocean Waves Breaking and Marine Aerosol Fluxes, vol. 38 of *Atmospheric and Oceanographic Sciences Library*, Springer New York, doi:10.1007/978-0-387-69092-6, 2007a.

Massel, S. R.: Ocean Waves Breaking and Marine Aerosol Fluxes, vol. 38 of *Atmospheric and Oceanographic Sciences Library*, chap. 7, pp. 183–206, Springer New York, doi:10.1007/978-0-387-69092-6, 2007b.

Monahan, E. C. and Muircheartaigh, I. O.: Optimal Power-Law Description of Oceanic Whitecap Coverage Dependence on Wind Speed, J. Phys. Oceanogr., 10, 2094–2099, doi:10.1175/1520-0485(1980)010<2094:OPLDOO>2.0.CO;2, 1980.

Monahan, E. C., Spiel, D. E., and Davidson, K. L.: A Model of Marine Aerosol Generation via Whitecaps and Wave Disruption, pp. 167–174, Oceanographic Sciences Library, Springer, Dordrecht, Netherlands, doi:10.1007/978-94-009-4668-2_16, 1986.

Nenes, A., Pandis, S. N., and Pilinis, C.: ISORROPIA: A New Thermodynamic Equilibrium Model for Multiphase Multicomponent Inorganic Aerosols, Aquat. Geochem., 4, 123–152, doi:10.1023/A:1009604003981, 1998.

Nenes, A., Pandis, S. N., and Pilinis, C.: Continued development and testing of a new thermodynamic aerosol module for urban and regional air quality models, Atmos. Environ., 33, 1553 – 1560, doi:10.1016/S1352-2310(98)00352-5, 1999.

Neumann, D., Matthias, V., Bieser, J., Aulinger, A., and Quante, M.: Sensitivity of modeled atmospheric nitrogen species to variations in sea salt emissions in the North and Baltic Sea regions, Atmospheric Chemistry and Physics Discussions, 15, 29 705–29 745, doi:10.5194/acpd-15-29705-2015, 2015.

O'Dowd, C. D. and de Leeuw, G.: Marine aerosol production: a review of the current knowledge, Philos. T. Roy. Soc. A, 365, 1753–1774, doi:10.1098/rsta.2007.2043, 2007.

Otte, T. L. and Pleim, J. E.: The Meteorology-Chemistry Interface Processor (MCIP) for the CMAQ modeling system: updates through MCIPv3.4.1, Geosci. Model Dev., 3, 243–256, doi:10.5194/gmd-3-243-2010, 2010.

Ovadnevaite, J., Manders, A., de Leeuw, G., Ceburnis, D., Monahan, C., Partanen, A.-I., Korhonen, H., and O'Dowd, C. D.: A sea spray aerosol flux parameterization encapsulating wave state, Atmos. Chem. Phys., 14, 1837–1852, doi:10.5194/acp-14-1837-2014, 2014.

Petelski, T., Markuszewski, P., Makuch, P., Jankowski, A., and Rozwadowska, A.: Studies of vertical coarse aerosol fluxes in the boundary layer over the Baltic Sea*, Oceanologia, 56, 697 – 710, doi:10.5697/oc.56-4.697, 2014.

Salter, M. E., Zieger, P., Acosta Navarro, J. C., Grythe, H., Kirkevåg, A., Rosati, B., Riipinen, I., and Nilsson, E. D.: An empirically derived inorganic sea spray source function incorporating sea surface temperature, Atmos. Chem. Phys., 15, 11 047–11 066, doi:10.5194/acp-15-11047-2015, 2015.

Sarwar, G., Luecken, D., and Yarwood, G.: Chapter 2.9 Developing and implementing an updated chlorine chemistry into the community multiscale air quality model, in: Air Pollution Modeling and Its Application XVIII, edited by Borrego, C. and Renner, E., vol. 6 of *Developments in Environmental Science*, pp. 168 – 176, Elsevier, Amsterdam, Netherlands, doi:10.1016/S1474-8177(07)06029-9, 2007.

Seinfeld, J. H. and Pandis, S. N.: Atmospheric Chemistry and Physics: From Air Pollution to Climate Change, chap. 10, Wiley-Interscience, Hoboken, New Jersey, 2nd edn., 2006.

Sharqawy, M. H., Lienhard, J. H., and Zubair, S. M.: Thermophysical properties of seawater: a review of existing correlations and data, Desalination and Water Treatment, 16, 354–380, doi:10.5004/dwt.2010.1079, 2010.

Smith, M. H., Park, P. M., and Consterdine, I. E.: Marine aerosol concentrations and estimated fluxes over the sea, Q. J. Roy. Meteor. Soc., 119, 809–824, doi:10.1002/qj.49711951211, 1993.

Spada, M., Jorba, O., Pérez García-Pando, C., Janjić, Z., and Baldasano, J. M.: Modeling and evaluation of the global sea-salt aerosol distribution: sensitivity to size-resolved and sea-surface temperature dependent emission schemes, Atmos. Chem. Phys., 13, 11 735–11 755, doi:10.5194/acp-13-11735-2013, 2013.

Tanaka, P. L., Allen, D. T., McDonald-Buller, E. C., Chang, S., Kimura, Y., Mullins, C. B., Yarwood, G., and Neece, J. D.: Development of a chlorine mechanism for use in the carbon bond IV chemistry model, J. Geophys. Res. Atmos., 108, 4145, doi:10.1029/2002JD002432, 2003.

Tang, I. N., Tridico, A. C., and Fung, K. H.: Thermodynamic and optical properties of sea salt aerosols, J. Geophys. Res. Atmos., 102, 23 269–23 275, doi:10.1029/97JD01806, 1997.

Tørseth, K., Aas, W., Breivik, K., Fjæraa, A. M., Fiebig, M., Hjellbrekke, A. G., Lund Myhre, C., Solberg, S., and Yttri, K. E.: Introduction to the European Monitoring and Evaluation Programme (EMEP) and observed atmospheric composition change during 1972-2009, Atmos. Chem. Phys., 12, 5447–5481, doi:10.5194/acp-12-5447-2012, 2012.

Tsyro, S., Aas, W., Soares, J., Sofiev, M., Berge, H., and Spindler, G.: Modelling of sea salt concentrations over Europe: key uncertainties and comparison with observations, Atmos. Chem. Phys., 11, 10 367–10 388, doi:10.5194/acp-11-10367-2011, 2011.

Weisse, R., Bisling, P., Gaslikova, L., Geyer, B., Groll, N., Hortamani, M., Matthias, V., Maneke, M., Meinke, I., Meyer, E. M., Schwichtenberg, F., Stempinski, F., Wiese, F., and Wöckner-Kluwe, K.: Climate services for marine applications in Europe, Earth Perspectives, 2, 1–14, doi:10.1186/s40322-015-0029-0, 2015.

Whitten, G. Z., Heo, G., Kimura, Y., McDonald-Buller, E., Allen, D. T., Carter, W. P., and Yarwood, G.: A new condensed toluene mechanism for Carbon Bond: CB05-TU, Atmos. Environ., 44, 5346 – 5355, doi:10.1016/j.atmosenv.2009.12.029, atmospheric Chemical Mechanisms: Selected Papers from the 2008 Conference, 2010.

Wu, J.: Wind-stress coefficients over sea surface from breeze to hurricane, J. Geophys. Res.-Oceans, 87, 9704–9706, doi:10.1029/JC087iC12p09704, 1982.

Yarwood, G., Rao, S., Yocke, M., and Whitten, G. Z.: Updates to the Carbon Bond Chemical Mechanism: CB05, Final report to project rt-04-00675, U.S. Environmental Protection Agency, Research Triangle Park, NC 27703, 2005.

Zhang, K. M., Knipping, E. M., Wexler, A. S., Bhave, P. V., and Tonnesen, G. S.: Size distribution of sea-salt emissions as a function of relative humidity, Atmos. Environ., 39, 3373 – 3379, doi:10.1016/j.atmosenv.2005.02.032, 2005.

Atmos. Chem. Phys. Discuss., doi:10.5194/acp-2015-946, 2016
Manuscript under review for journal Atmos. Chem. Phys.
Published: 23 February 2016

Atmospheric Chemistry and Physics Discussions

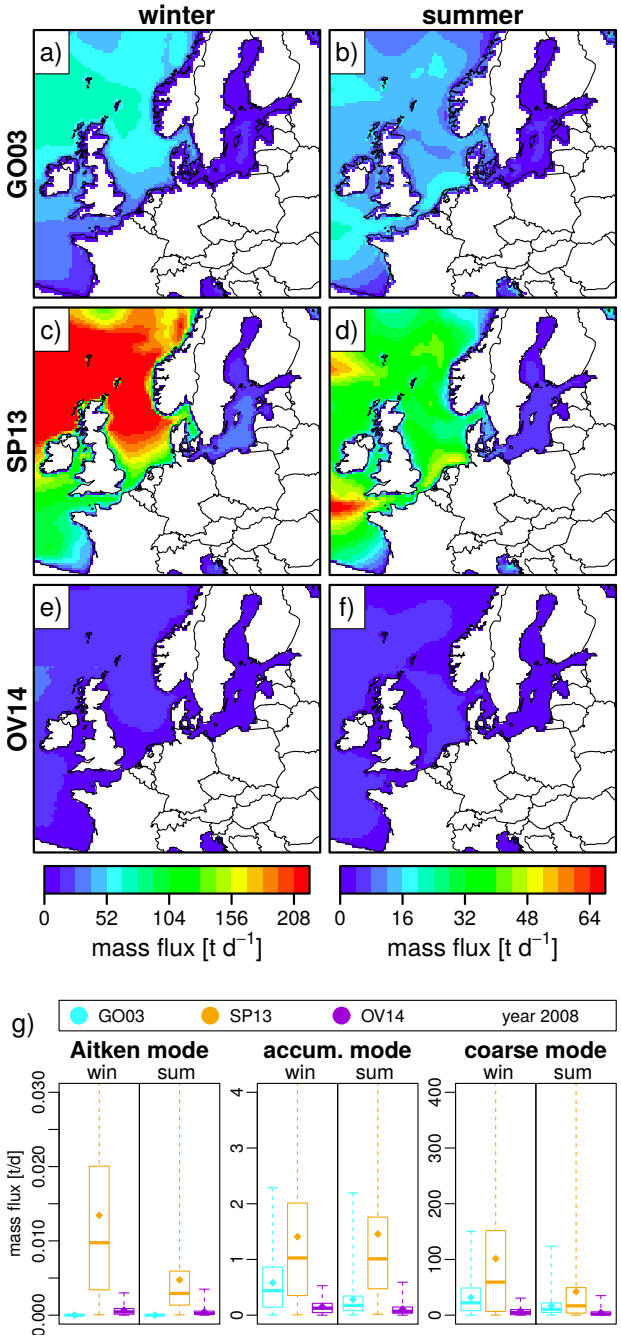

Figure 6. Sea salt mass emissions in tons of sea salt per day and grid cell $\left[\mathrm{t\ d^{-1}}\right]$ (total mass of sea salt and not mass of sodium). **a-f**: two-month average mass emissions in winter (left column) and summer (right column). The emissions were calculated using the GO03, SP13, and OV14 (top to bottom) emission parameterizations. The color scale is the same for all plots in the same column. **g**: box plots of mass emissions in the Aitken, accumulation and coarse modes (left to right) at one location in the German Bight (Fig. 5) during summer and winter 2008.

Atmos. Chem. Phys. Discuss., doi:10.5194/acp-2015-946, 2016
Manuscript under review for journal Atmos. Chem. Phys.
Published: 23 February 2016

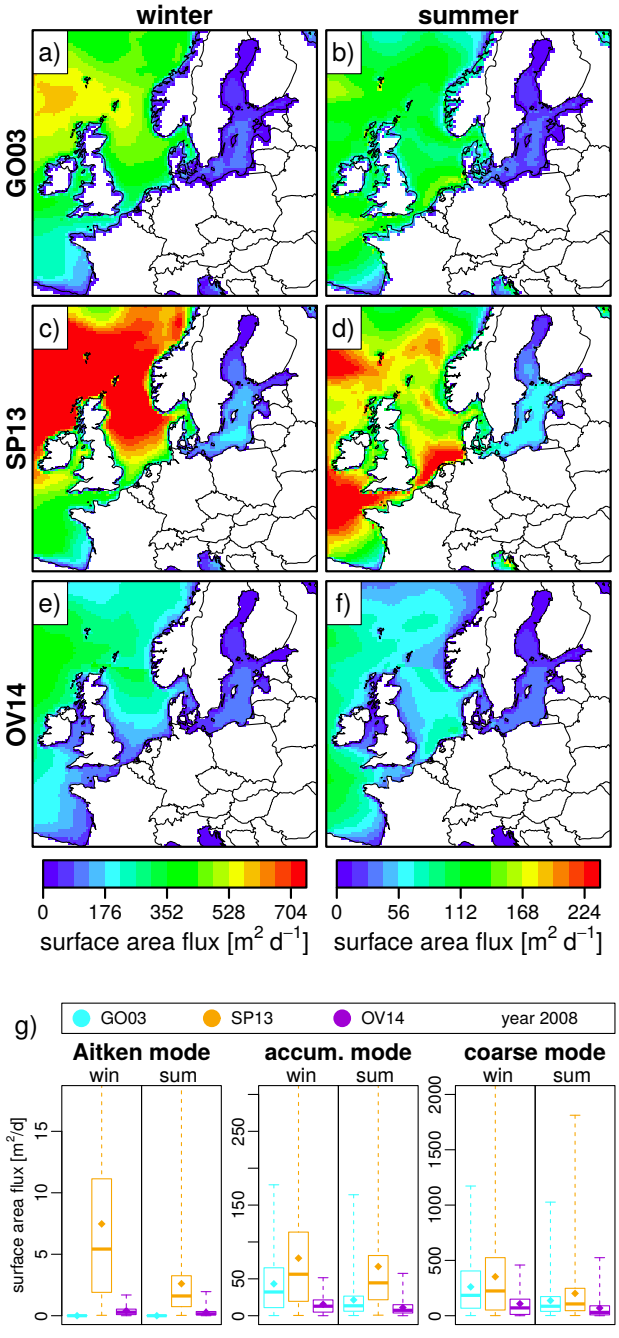

Figure 7. Similar to Fig. 6 but showing sea salt surface area emissions. **a-f**: two-month average surface area emissions **g**: box plots of surface area emissions.

Atmos. Chem. Phys. Discuss., doi:10.5194/acp-2015-946, 2016
Manuscript under review for journal Atmos. Chem. Phys.
Published: 23 February 2016

Atmospheric Chemistry and Physics Discussions

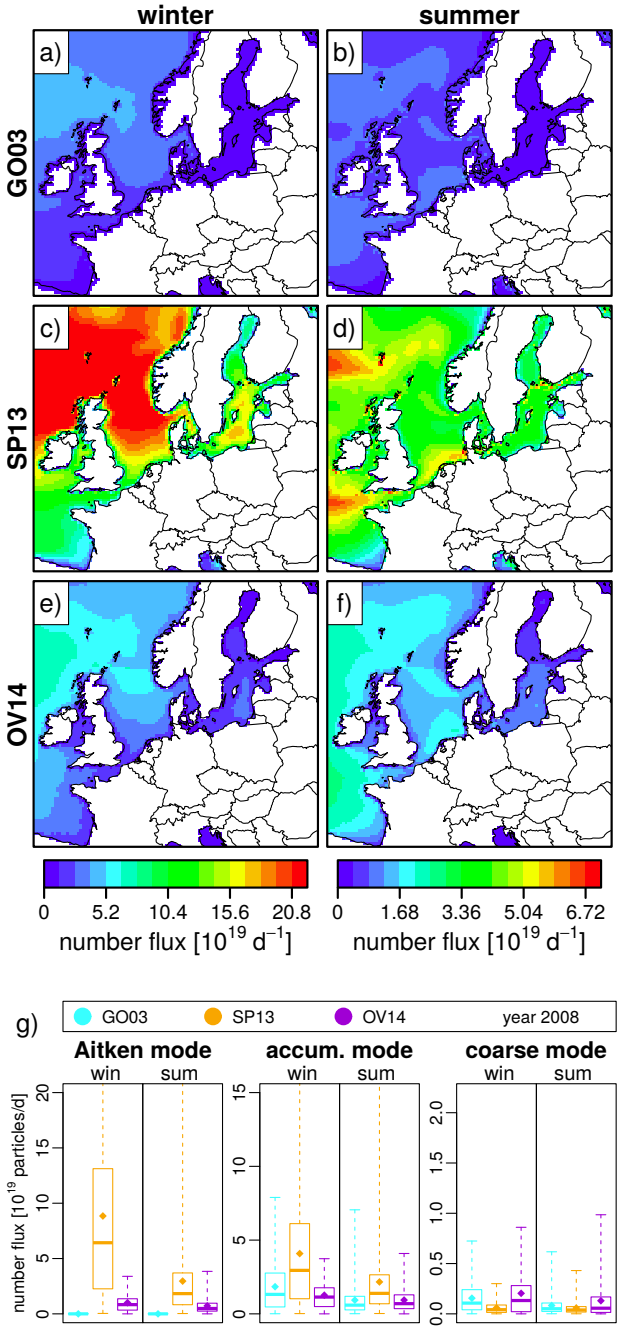

Figure 8. Similar to Fig. 6 but showing sea salt number emissions. **a-f**: two-month average number emissions **g**: box plots of number emissions.

Atmos. Chem. Phys. Discuss., doi:10.5194/acp-2015-946, 2016
Manuscript under review for journal Atmos. Chem. Phys.
Published: 23 February 2016

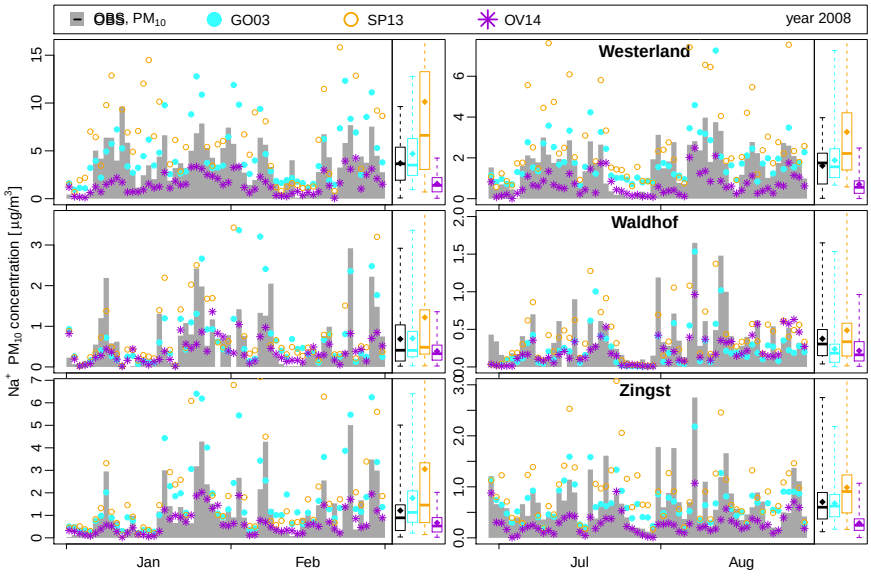

Figure 9. Sodium concentrations at three representative EMEP stations (Westerland, Waldhof and Zingst). The black box plot represents the observations. For the box plots of the modeled data, only the daily model values with corresponding measured values are considered.

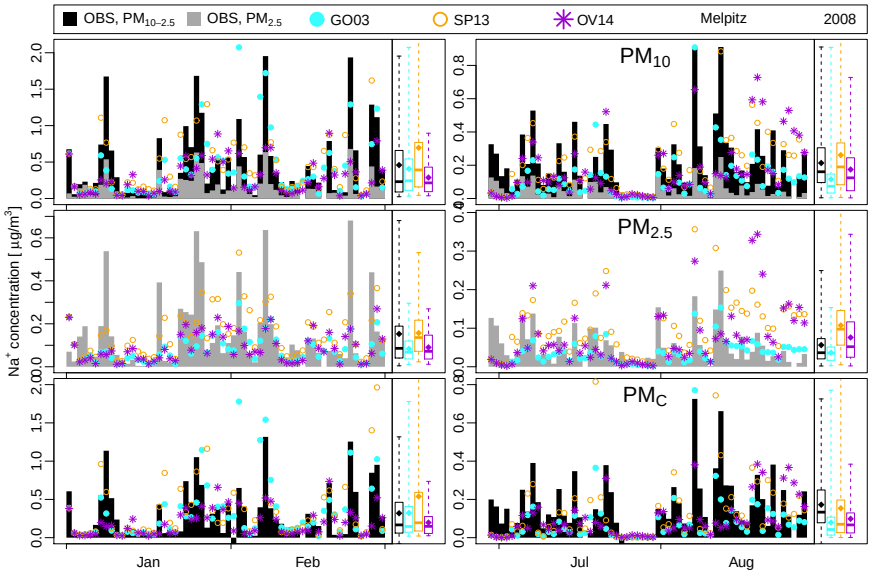

Figure 10. Daily average measured and modeled sodium concentrations at the EMEP station at Melpitz. The PM_{10}, $PM_{2.5}$ and PM_C concentrations are plotted in the top, center and bottom rows, respectively, for winter (left) and summer (right). The black box plot represents the observations. For the box plots of the modeled data, only the daily model values with corresponding measured values are considered.

Atmos. Chem. Phys. Discuss., doi:10.5194/acp-2015-946, 2016
Manuscript under review for journal Atmos. Chem. Phys.
Published: 23 February 2016

Atmospheric Chemistry and Physics Discussions

Table 3. Statistical evaluation for the comparisons between the modeled and measured Na^+ concentrations at 11 EMEP stations in the vicinity of the North and Baltic Seas during winter (left) and summer (right).

Station	Case	winter				summer			
		n	RAE	MNB	R	n	RAE	MNB	R
Westerland	GO03	60	1.89	1.01	0.76	61	0.72	2.37	0.70
DE0001R	SP13	60	6.75	2.22	0.71	61	1.83	3.36	0.73
Coast	OV14	60	2.21	-0.36	0.75	61	1.00	-0.11	0.70
Waldhof	GO03	55	0.42	1.75	0.67	60	0.18	-0.33	0.70
DE0002R	SP13	55	0.75	2.27	0.76	60	0.25	0.36	0.71
Inland	OV14	55	0.39	0.64	0.73	60	0.20	-0.34	0.68
Neuglobsow	GO03	60	0.30	1.27	0.76	59	0.18	-0.36	0.71
DE0007R	SP13	60	0.66	1.71	0.83	59	0.18	0.32	0.72
Inland	OV14	60	0.35	0.43	0.77	59	0.19	-0.32	0.65
Zingst	GO03	60	0.72	1.24	0.79	61	0.26	0.20	0.69
DE0009R	SP13	60	1.91	1.85	0.81	61	0.46	0.69	0.59
Coast	OV14	60	0.63	-0.09	0.77	61	0.43	-0.56	0.76
Melpitz	GO03	59	0.25	0.43	0.66	61	0.11	-0.35	0.69
DE0044R	SP13	59	0.39	1.27	0.67	61	0.12	0.58	0.67
Inland	OV14	59	0.27	0.11	0.65	61	0.13	0.12	0.57
Tange	GO03	56	1.03	1.12	0.67	61	0.44	0.88	0.65
DK0003R	SP13	56	2.97	2.03	0.74	61	0.84	1.22	0.74
Inland	OV14	56	0.96	-0.22	0.73	61	0.44	-0.32	0.67
Keldsnor	GO03	60	1.26	0.75	0.48	56	0.46	0.21	0.26
DK0005R	SP13	60	2.91	1.19	0.68	56	0.76	0.51	0.37
Coast	OV14	60	1.31	-0.50	0.46	56	0.75	-0.63	0.39
Anholt	GO03	59	1.26	0.51	0.81	51	0.60	0.05	0.69
DK0008R	SP13	59	4.44	1.49	0.82	51	0.91	0.31	0.68
Coast	OV14	59	1.61	-0.53	0.71	51	1.07	-0.67	0.59
Ulborg	GO03	60	1.41	1.63	0.77	54	0.68	1.22	0.52
DK0031R	SP13	60	4.87	1.82	0.83	54	1.15	1.07	0.79
Coast	OV14	60	1.33	-0.33	0.79	54	0.62	-0.40	0.71
Utö	GO03	59	0.59	1.26	0.59	61	0.24	0.24	0.67
FI0009R	SP13	59	1.86	3.10	0.64	61	0.33	0.91	0.64
Coast	OV14	59	0.32	0.23	0.61	61	0.33	-0.30	0.57
Virolahti II	GO03	60	0.24	1.50	0.37	54	0.09	0.16	0.75
FI0017R	SP13	60	0.50	2.71	0.49	54	0.13	1.10	0.72
Coast	OV14	60	0.18	0.74	0.33	54	0.12	0.34	0.55

Atmos. Chem. Phys. Discuss., doi:10.5194/acp-2015-946, 2016
Manuscript under review for journal Atmos. Chem. Phys.
Published: 23 February 2016

Atmospheric Chemistry and Physics Discussions

Table 4. Similar to Table 3 but for the Melpitz station only and for different particle sizes.

Size	Case	winter				summer			
		n	RAE	MNB	R	n	RAE	MNB	R
PM_{10}	GO03	59	0.25	0.43	0.66	61	0.11	-0.35	0.69
	SP13	59	0.39	1.27	0.67	61	0.12	0.58	0.67
	OV14	59	0.27	0.11	0.65	61	0.13	0.12	0.57
$PM_{2.5}$	GO03	58	0.09	0.19	0.64	56	0.03	0.08	0.50
	SP13	58	0.10	1.37	0.64	56	0.07	2.28	0.45
	OV14	58	0.10	0.39	0.52	56	0.06	1.27	0.31
PM_C [a]	GO03	56	0.20	0.69	0.64	52	0.11	-0.40	0.53
	SP13	56	0.35	1.42	0.65	52	0.13	0.15	0.50
	OV14	56	0.19	0.19	0.65	52	0.11	-0.27	0.48

[a] PM_C is calculated as $PM_{10}-PM_{2.5}$. In rare situations, $PM_{10}<PM_{2.5}$ exists in the measurements. In these situations, the resulting PM_C value is not considered.

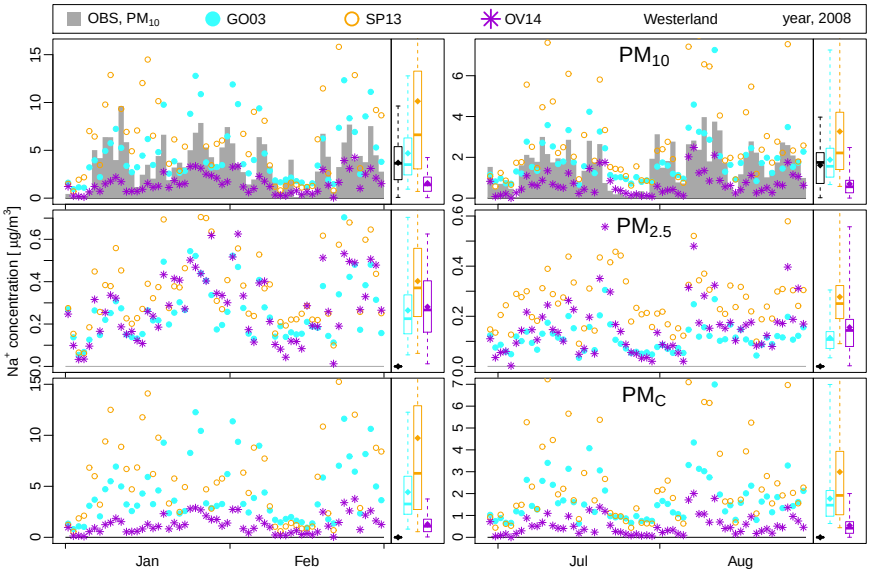

Figure 11. Similar to Fig. 10 but showing data for Westerland. No $PM_{2.5}$ data were available and no PM_C concentrations were calculated.

Atmos. Chem. Phys. Discuss., doi:10.5194/acp-2015-946, 2016
Manuscript under review for journal Atmos. Chem. Phys.
Published: 23 February 2016

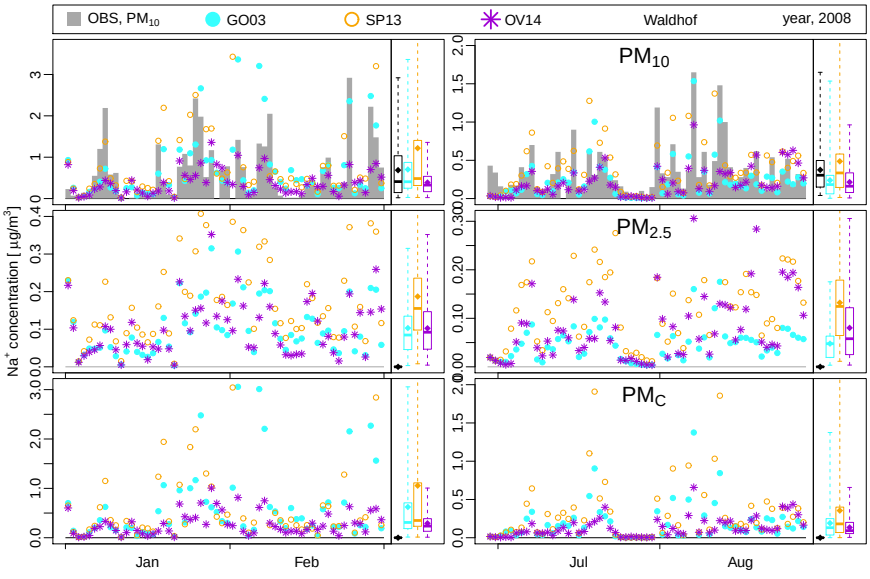

Figure 12. Similar to Fig. 10 but showing data for Waldhof. No $PM_{2.5}$ data were available nd no PM_C concentrations were calculated.

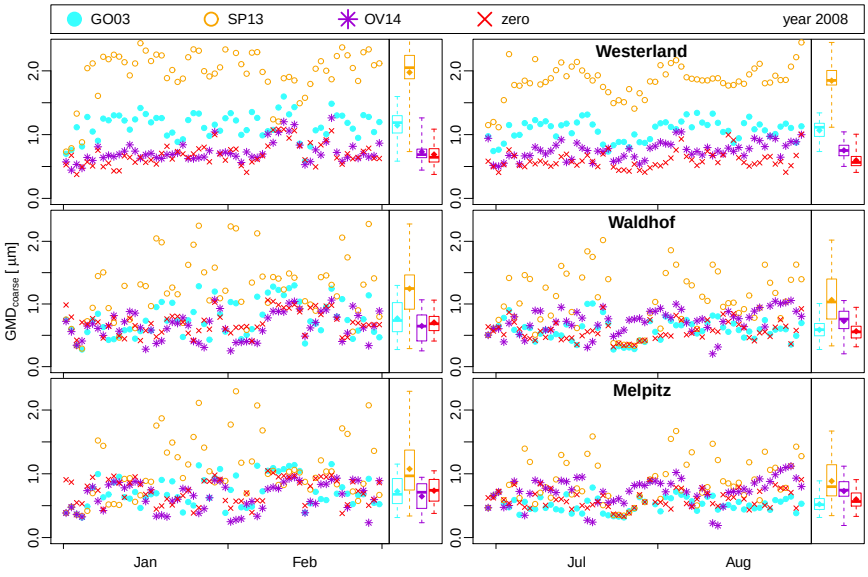

Figure 13. Similar to Fig. 9 but showing the GMDs of the modeled coarse-mode particle distributions. Not only sodium or sea salt but all coarse mode species are considered.

Atmos. Chem. Phys. Discuss., doi:10.5194/acp-2015-946, 2016
Manuscript under review for journal Atmos. Chem. Phys.
Published: 23 February 2016

Atmospheric Chemistry and Physics Discussions

Table 5. Parameters, their units and their meaning.

Parameter	Unit	Explanation
r_{80}	µm	particle radius at 80% relative humidity
D_{dry}	µm	dry particle diameter
PM_{10}	µg m^{-3}	total particle mass
$\text{PM}_{2.5}$	µg m^{-3}	fine particle (≤ 2.5 µm) mass, $\neq \sum$ CMAQ Aitken- and accumulation-mode mass
PM_{C}	µg m^{-3}	coarse particle mass: $\text{PM}_{10}-\text{PM}_{2.5}$, $\neq$ CMAQ coarse-mode mass
u_{10}	m s^{-1}	10 m wind speed
SST	K	sea surface temperature
SAL	‰	sea surface salinity
W	-	whitecap coverage between 0 (0%) and 1 (100%)
u_*	m s^{-1}	friction velocity at the sea surface
H_S	m	significant wave height
C_D	-	drag coefficient due to wind waves
ν_W	m^2 s^{-1}	sea water kinetic viscosity
Re_{Hw}	-	Reynolds number of the sea surface due to waves
RH	%	relative humidity
GMD	µm	geometric mean diameter
σ	-	standard deviation
$\frac{dF}{dr_{80}}$, $\frac{dF}{dD_{\text{dry}}}$	$\frac{\text{number}}{\text{m}^2\ \mu\text{m}\ \text{s}}$	particle number flux
$\frac{dF}{d\log D_{\text{dry}}}$	$\frac{\text{number}}{\text{m}^2\ \text{s}}$	particle number flux
ρ_{ss}	g cm^{-3}	density of dry sea salt